Chapter 2
Methods and Structures for Self-assembly of Anisotropic 1D Nanocrystals

Shuang-Yuan Zhang, Kwok Wei Shah and Ming-Yong Han

Abstract In the nanoscience and nanotechnology, the study of nanocrystal self-assembly has been regarded as a key technology in leading future industrial development. The colloidal self-assembly techniques, particularly for one-dimensional (1D) building blocks, have been widely adopted for the systematic fabrication of functional nanocrystals and received an extensive research attention. However, the increase in the building blocks' anisotropy, e.g. from sphere to rod/wire, has dramatically leveled up the difficulty in organizing them into ordered structures. To realize tailored 1D nanocrystal self-assembled structures, a profound understanding and detailed design of self-assembly mechanism and procedures are much needed. Here, a thorough review over 1D nanocrystal self-assembly methods and alignments are present to achieve large-scale functional structures. Through different techniques, such as evaporation, template, electric field, Langmuir-Blodgett film and chemical bonding, nanocrystals with various shapes can be self-assembled on substrates, at interfaces and in solutions. These assembled structures that have been achieved so far, can exhibit different degrees of alignments, such as stripe pattern as non-close-packed structure, horizontal, vertical alignments as close-packed monolayers, nematic, semectic alignments, AB stacking of vertical alignments, three-dimensional (3D) assembly as close-packed multilayers. In general, these self-assembly techniques can reach much small dimension and create microstructures that possess unique properties different from their individual building blocks.

S.-Y. Zhang (✉) · K.W. Shah · M.-Y. Han (✉)
Institute of Materials Research and Engineering, Agency for Science, Engineering and Research, 3 Research Link, 117602 Singapore, Singapore
e-mail: zhangs@imre.a-star.edu.sg

M.-Y. Han
e-mail: my-han@imre.a-star.edu.sg

© Springer International Publishing Switzerland 2015

Q. Li (ed.), *Anisotropic Nanomaterials*, NanoScience and Technology,
DOI 10.1007/978-3-319-18293-3_2

2.1 Introduction

The past few decades have witnessed an enormous explosion in the research efforts in the nanoscience and nanotechnology: from synthesizing new nanomaterials to characterizing [1–9], understanding their unique chemical, physical, biological properties [10–18], and more recently to self-assembling these individual components into larger systems and structures [19–25]. The self-assembly of individual nanocrystals has provided a bottom-up method that reaches much smaller dimension. It is able to align, pattern, integrate nanocrystals into ordered and functional microscale structures that is inaccessible from top-down methods, e.g. lithography, nano imprinting [26–28]. The colloidal route of nanocrystal self-assembly is an alternative means of nanofabrication to develop efficient micro-sized devices in a simple and versatile manner [29]. More importantly, it offers an inexpensive approach to build up large structures with new functions that differ from their initial building blocks. These new collective properties of assembled structures are tunable upon varying size, morphology and composition of these building blocks as well as the packing order [30]. A variety of nanomaterials including metals [31–37], semiconductors [38, 39], oxides [40–42], inorganic salts [28, 43], and polymers [38, 44] have been achieved to be self-assembled into larger, ordered structures with new properties. These assembled structures provide new perspectives for the application in the photonics [45–50], plasmonics [51–53], SERS [54–59], devices and deliver revolutionary solutions for magnetics [16, 41, 60, 61], electronic/photovoltaic devices [62–64], catalysis and energy storage [65]. Many of these applications are based not only on individual nano-objects but also on assemblies in which these nano-objects interact with one another and organize in dedicated ways. Therefore, the ability to self-assemble various nanocrystals into large ordered structures with desired size, shape and orientation has become crucial in solving new challenges and problems in nanoscience and nanotechnology research.

The building blocks for ordered self-assembled structures, which have been achieved so far, are priced restrictive requirements to be mono-dispersed [66, 67]. Individual nanocrystals, often terms as “artificial atoms” can assemble into large, microscale supercrystal or ordered solid structure in a dynamic equilibrium process when prepared with high uniformity. Traditionally, the building blocks of most assemblies are limited to spherical nanoparticles, and are studied extensively using simple drop-casting method [68–73]. The face-centered cubic (*fcc*) or hexagonal close-packed (*hcp*) packing pattern are usually observed when drop-casting and drying the uniform spherical nanoparticle dispersion onto a flat surface. Recent advances put emphasis to improve drop-casting method, with careful control over the evaporation rate and the choice of carrier solution, to enable the near-spherical nanoparticles, e.g. cubic, octahedral to form close-packed assembled structures. However, the increase in the building blocks’ anisotropy is found dramatically level up the difficulties to assemble such nanocrystals into long-ranged ordered structure [74–76], and the conventional drop-casting method face complexities in

self-assembling one-dimensional (1D) high anisotropic nanostructures, such as nanorods, nanowires [74].

In addition, when the self-assembly building blocks become assorted, especially lD anisotropic nanocrystals are used to assemble ordered structures, the crystal orientations (facet orientation) of these nanocrystals within the assembled structure become a prominent issue and of fundamental and practical research interest. Unlike spherical nanocrystals fitting into *fcc* or *hcp* pattern with a random crystal facet orientation, some 1D anisotropic nanocrystals assemble into more complicated packing patterns with both positional and orientational orders that otherwise unattainable using spherical nanocrystals [20, 22, 74–77]. This is particularly significant for certain applications as assemblies consisting of anisotropic nanocrystals possess unique properties due to their anisotropic nature [78]. Therefore, a significant research attention is diverted to this field and different self-assembly approaches, e.g. evaporation-mediated method, electric-field-assisted assembly, and template-assisted assembly [26, 27, 79–85] have been developed to assemble 1D anisotropic nanocrystals into ordered structures.

In this chapter, we focus on self-assemblies using 1D nanoscale building blocks and assess various assembling methods and different packing structures. The recent approaches that achieve self-assemblies on substrates, at interfaces, and in solutions are categorized and illustrated with detailed working mechanisms and actual setups. The different packing structures, such as stripes, monolayers, and multilayers that are fabricated from 1D nanocrystals are listed in the following section, with the emphases on the internal organization and unique properties. The challenges that faced by the current research works are also discussed, hoping to offer an outlook into future development. The ultimate goal is to provide a channel to fine tune 1D nanocrystals self-assembly into desired structures that is both functional and accessible for microscale applications.

2.2 Self-assembly Methods

Monodispersed colloidal nanocrystals with uniform size and shape distribution can self-assemble into large and ordered structures in a dynamic process on substrate or at interface or even in the colloidal solutions via different approaches. The formation of ordered structures depends on the building blocks and assembly approaches. The 1D anisotropic nanocrystals are particularly difficult to self-assemble due to their anisotropic structure properties and therefore require specific techniques and external facilitations. Here we summarize the approaches that have been developed so far to assemble 1D colloidal nanocrystals especially nanorods and nanowires into ordered structures.

2.2.1 Self-assembly on Substrates

2.2.1.1 Evaporation-Mediated Assembly

The controlled evaporation-mediated assembly is derived from simple drop-casting method that has been widely used in self-assembling spherical and non-isotropic colloidal nanocrystals [86, 87] on solid substrates. The formation of ordered self-assembled nanostructures was first observed using TEM by drop-casting the ferrofluid ($Fe_{1-x}C_x$) solution on a TEM grid [88]. In general, when a drop of nanocrystals suspension is withdrawn to deposit onto a flat substrate, as the carrier solvent is slowly evaporated, the nanocrystals self-assembled into ordered structure on the substrate surface to minimize the free energy (Fig. 2.1a) [89]. The relatively weak attraction forces (electrostatic interaction, Van Der Waals force, capping ligands interaction, hydrophobic interaction, capillary force [29] among nanocrystals in the suspension gain importance when the solvent is slowly evaporated, forcing nanocrystals to organize [82]. This aggregation process is also well explained using thermodynamics [90] and phase segregation model [91, 92], where the formation of final ordered structure depends on temperature, concentration, choices of solvent, nanoparticles sizes and thermodynamic state. Therefore, when the simple drop-casting method faces difficulty in self-assembling 1D anisotropic nanocrystals, different approaches that control the evaporation parameters such suspension concentration, choice of carrier solvent, evaporation rate have been proposed and demonstrated in anisotropic nanocrystals assembly.

To self-assemble 1D nanocrystals into ordered structures, the as-prepared nanocrystals are usually first subjected to a post-reaction treatment to narrow the size distribution. Most often, a non-solvent is added into stock solution with stirring until the initially homogeneous solution become turbid [81]. The large nanocrystals aggregate and precipitate at low centrifugation speed while the small sized nanocrystals remain in the supernatant. To further screening nanocrystals, additional non-solvent is added into the supernatant and another size selection can be carried out with a higher centrifugation speed. The above process is repeated until desired size distribution is reached. The size selection can also be carried out using filtration instead of centrifugation.

For the preparation of nanocrystal self-assemblies via controlled evaporation, the resulting uniform nanocrystals are dispersed into appropriate solvent with desired nanocrystal concentration. The concentration and choice of stabilizing surfactant can be adjusted by centrifugation, re-dispersion and ligand-exchange to avoid disordered aggregation [93, 94]. The surfactant concentration in the nanocrystal dispersions has to be larger than a critical value for the formation of ordered superstructures. This critical concentration appears to correspond to the amount of surfactant required to form a bilayer on the nanocrystal surface. Au nanorods without the surfactant bilayer coating tend to aggregate in a disordered manner because of the large van der Waals attraction (Au–Au Hamaker constant $A \approx 1.95$ eV) [95]. A minimum surfactant concentration is therefore required to

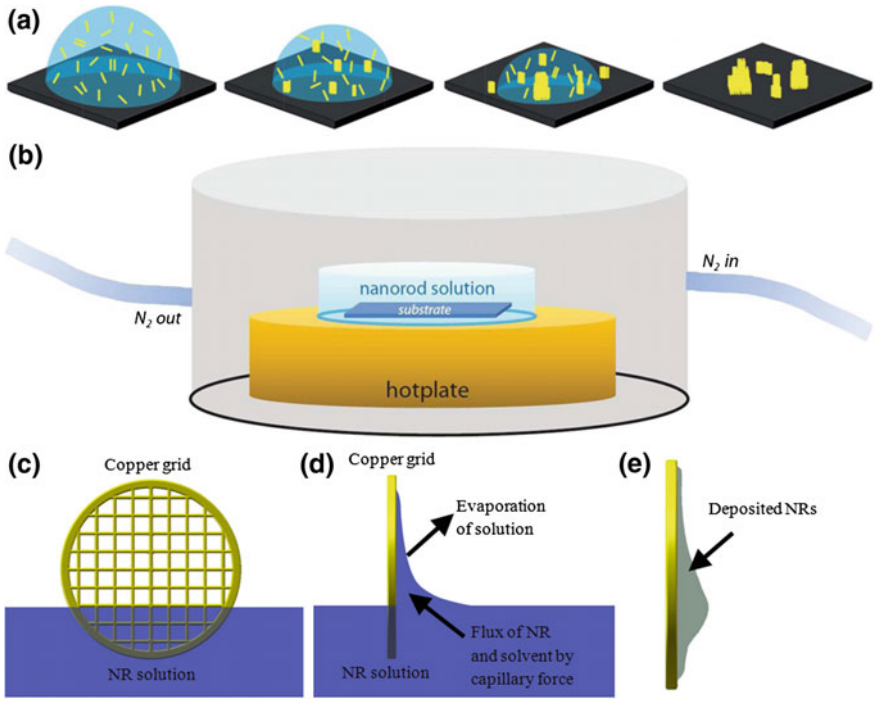

Fig. 2.1 Evaporation-mediated assembly. **a** Schematics showing the progression of evaporation-mediated assembly: the initial random distribution of nanorods, self-assembly during evaporation, formation of small assemblies, and final deposition of large-area assembled structures. Reproduced with permission from [89]. **b** Schematic diagram of an evaporation-mediated assembly setup. The substrate is placed in the *bottom* of a short-walled container, which is filled with 1D nanocrystal solution. This container is set on a hotplate, and placed inside a small Teflon evaporation chamber. A controlled flow rate of dry nitrogen through the small atmosphere of the chamber enables control of solvent evaporation rate. Reproduced with permission from [93]. **c–e** Schematics of the deposition method in evaporation-mediated assembly. **c** A TEM grid is inserted about 1/4 of the diameter into the Au nanorod solution. A thin film of solution is formed due to the capillary action. **d** Evaporation of water from the thin film causes influx of water and nanorods. **e** The accumulation of nanocrystals leads to the formation of self-assembled structures. Reproduced with permission from [96]

maintain the balance between the entropic depletion potential and electrostatic repulsion potential for the formation of nanorod superstructures [94].

A typical setup for controlled evaporation is shown in Fig. 2.1b, in which the solvent was evaporated with a fine control. A drop (5–10 mL) of 1D nanocrystal dispersion was placed onto a clean flat substrate, e.g. silicon, silicon nitride. The droplet was kept undisturbed at a particular temperature (usually 30–60 °C depends on the chosen solvent's boiling point and desired evaporation rate) for a constant evaporation rate. Higher temperature above 60 °C was reported to cause disordered assemblies as the evaporation was too fast for the nanorods to attain their equilibrium positions. The humidity of the evaporation chamber was also under

carefully control for a constant evaporation rate. In often cases, approximately 60 % humidity caused by water or solvent was maintained during the evaporation [94]. Very slow evaporation rate which took several hours was usually adopted in self-assembling 1D nanocrystals and found helpful to increase packing order and assembled structure size. The evaporation chamber could also be supplied with a controlled flow of dry nitrogen either under atmosphere or under reduced pressure. The final assembled structures were shown related to concentration of 1D nanocrystal dispersions. Different nanorod concentrations were tested. The use of relatively concentrated solutions resulted in well-ordered nanorod assemblies, whereas the use of dilute solutions did not favor the formation of ordered assemblies.

The evaporation can also be controlled by capillary action in a much simple setup. The capillary force is able to induce a flow (solvent and nanocrystal) from solution to the substrate and create a thin film on the substrate. The solvent flux compensates the evaporated solvent from the film; while the nanocrystal flux causes nanocrystal accumulation and results in the self-assembled structures. El-Sayed and co-workers [96] have described an immersion method in controlling the evaporation so as to grow self-assembled structures from Au nanorods. In a general scenario, a flat substrate (a carbon-coated copper gird for instance) was vertically inserted partially into Au nanorod solution with the bottom part of gird immersed in the solution (Fig. 2.1c–e). Drying of the colloidal solution over 8 h led to the formation of reproducible self-assembled structures in most regions of the substrate. The immersion of substrate in colloidal solution first created a thin film on the substrate. The gentle evaporation of solvent from the thin film increased the lateral capillary forces between nanorods and built up a pressure gradient. This caused the influx of water and nanorods, and finally led to the packing of nanorods at the contact interface of the solution and substrate. It was shown that the immersion method could produce self-assemblies with high quality and factors such as the rate of water evaporation, the ionic strength, the surfactant concentration, and the particle size and shape distributions were important in this process.

2.2.1.2 Electric-Field-Assisted Assembly

In colloidal system, the external electric field has long been found to induce or strengthen the interactions between the nanocrystals and/or their capping ligands [97]. For 1D nanocrystals (including their capping ligands) carrying free electrons or with strong dipole moment, the electric field is a perfect stimulus in directing their assembly into a desire pattern and orientation [48, 76, 98–104]. These 1D nanocrystals are usually polarized along their longitudinal axes and experienced forces exerted by the electric field in the field streamline direction. When the electric-field-induced interactions are sufficiently strong to overcome Brownian motion, 1D nanocrystals can move along the electric field streamline and form a well-ordered structures with little defects and increased symmetry [102, 105]. A simple model can be established by considering thermal energy to evaluate the energy input in order to align 1D nanocrystals into ordered structures.

The electric-field-induced alignment energy are required to overcome thermal energy at room temperature $k_B T = 26$ meV (k_B is the Boltzmann constant) that would otherwise randomize the orientation of the 1D nanocrystals [100, 101]. On the basis of this, the minimum external electric field strength, lower bound of free electron density or dipole moment magnitude of nanocrystals can be determined when assembling the 1D nanocrystals.

In general, both direct current (DC) and alternating current (AC) electric field can be used as the external field in assisting 1D nanocrystals assembly. The nanorods or nanowires are able to be aligned uniformly over areas on the scale of several tens of square micrometers by following the electric field streamlines. In the case of DC electric-field-assisted assembly, a non-conducting flat surface, e.g. Si_3N_4, is used as the substrate and a pair of electrodes are placed either on the two sides of the substrate (left-right manner, Fig. 2.2a) or in a top-down manner (Fig. 2.2b). The placement of the electrodes determines the electric field direction and thus decides the assembled 1D nanocrystals orientation: perpendicular (top-down manner) or parallel (left-right manner) to the substrate. A drop of colloidal 1D nanocrystals solution is deposited on the substrate for a slow evaporation over a period of several hours that depends on the solvent vapor pressure and environment. A direct voltage **V** is applied simultaneously during the solvent evaporation, the magnitude of which has to produce alignment energy larger than thermal energy at room temperature ($k_B T$) as discussed above. The DC electric-field-assisted is a voltage-magnitude-dependent process and forces a high concentration of 1D nanocrystals inside the gap between two electrodes. In fact, the 1D nanocrystals concentration distribution contour strongly resembles that of electric field strength, where the nanocrystals concentration is highest around the electrodes [101].

The AC electric-field-assisted assembly shares a similar setup as that of DC electric field, with the change of alternating voltage applied at the electrodes. An electrically insulated electrode structure that consists of multiple interdigitated fingers pattern can be used to scale-up the assembly ability (Fig. 2.2c–e). The interdigitated electrode structures are fabricated by optical lithography and subsequent metal evaporation onto a Si/SiO_2 substrate with sizes and spacings in the order of a few microns [48, 76, 98]. The use of the AC electric field for the self-assembly avoids charging effect and excessive accumulation of the 1D nanocrystals around the electrodes [48]. Besides, it prevents the interference of electro-osmotic and electro-chemical effects that present in the DC system [82]. Different from the DC electric-field-assisted assembly, in which the applied voltage magnitude is the major parameter in controlling the assembly; in the case of AC circuit, the frequency of the alternating voltage also plays a role in assembling the 1D nanocrystals. In general, as the frequency of the AC circuit increases, the assembling time to form order assembled structure decreases. The high frequency prevents the polar molecules in the solvent to reorient in the rapidly changed electric filed because of their long relaxation times. This results in greater net polarization of the 1D nanocrystals and stronger alignment forces and thus shorter assembling time [106].

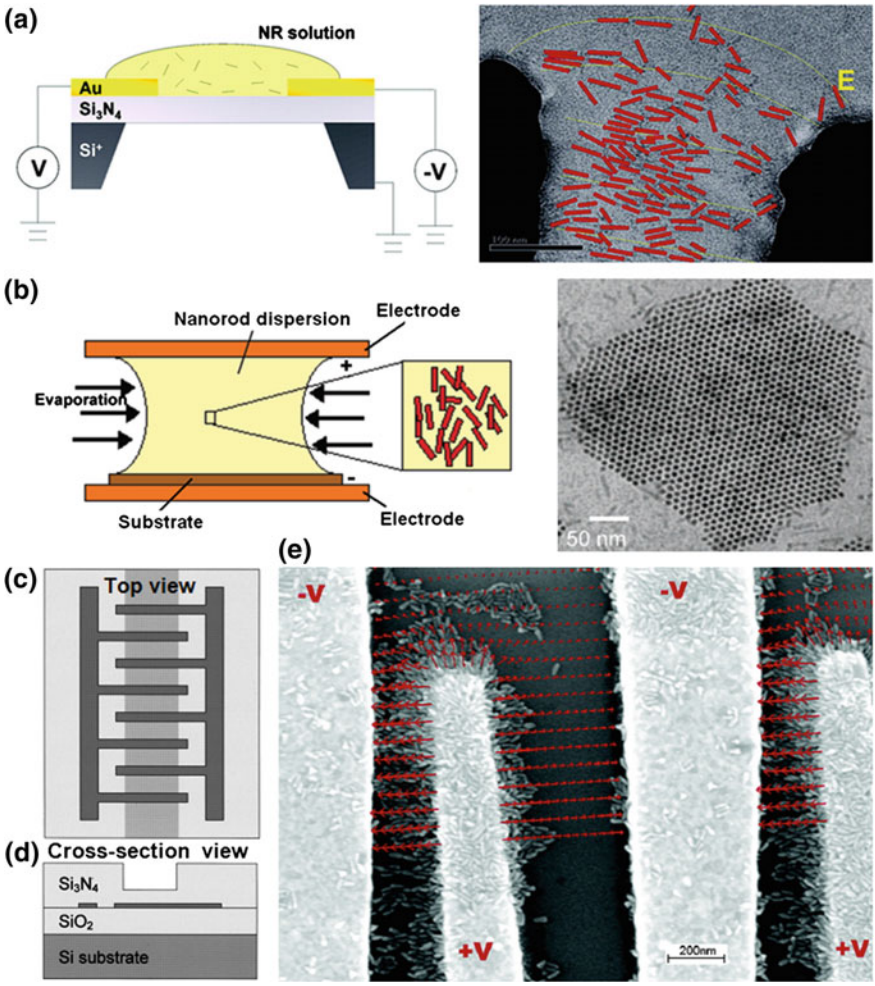

Fig. 2.2 External-field-assisted assembly. **a**, **b** Schematic representations of the experimental set-ups used in the assembly of colloidal cadmium chalcogenide nanorods under DC electric fields. **a** When the parallel electrodes (Au) are arranged in a coplanar manner, the nanorods are aligned in the plane of the substrate. The TEM image shows CdSe nanorods (shown as *red bars*) aligned along the electric field streamlines (shown in *yellow*). Reproduced with permission from [101]. **b** A *top-down* arrangement of the electrodes results in nanorods that are oriented perpendicular to the substrate. The TEM image shows perpendicularly aligned CdS nanorods. Reproduced with permission from [102]. **c** *Top* and **d** cross-sectional views of the multiple electrode structures used in the AC electric-field-assisted assembly. The interdigitated electrode fingers are placed on the SiO_2/Si substrate and covered with Si_3N_4 layer to prevent short circuit. Reproduced with permission from [98]. **e** SEM image showing nanorods accumulate in the region of strongest electric field and aligned along the electric field streamlines. Reproduced with permission from [48]

2.2.1.3 Template-Assisted Assembly

For colloidal nanocrystal self-assembling with a template, the template geometry and surface chemistry play an important role by incorporating active sites for nanocrystal selective deposition [107–111]. Modulating the geometry and surface chemistry of templates therefore offers a convenient tool in assisting 1D nanocrystal assembly. These templates can serve as hosts to accommodate 1D nanocrystals and allow the creation of ordered structures [75, 112–116]. For instance, conventional photo lithography permits patterning a substrate's surface with precise spatial and chemical control. This surface-modified substrate contains geometrically constrained sites and/or chemically active groups that induce the selective deposition of nanocrystals onto substrate with desired pattern. It shall be noted that other than the surface-modified substrates, biological molecules, e.g. DNA, peptides [117–123], microstructures, e.g. carbon nanotubes [124] or block copolymers [125–128], can also be considered as template in a broad sense. These molecules or structures provide a platform onto which nanocrystals are aligned into ordered structures that is complementary to themselves, through the covalent or non-covalent interactions.

The geometrically constrained template is a straightforward method that can create different assembly patterns. The pattern feature size and morphology put strict restrictions on how 1D nanocrystal deposit onto the surface. Due to the anisotropic nature of 1D nanocrystals, only certain orientations are accessible for their deposition (Fig. 2.3a–c). These templates need to be designed in accordance with building blocks. An excessive large feature sizes lead to disordered structures while a small feature sizes prevent the deposition of nanocrystals onto the template. The pattern feature sizes are generally in the same order of building blocks dimensions. For the case shown in Fig. 2.3a–c, to assembly CdSe nanorods with dimension around 35 × 7.5 nm into horizontal line alignment, a channel width of 30 nm can be used to selectively align these nanorods [114].

Other than geometrically constrained template, 1D nanocrystals can also be aligned on chemically active template. For instance, thiol groups tend to form colvent Au–S bonding with Au nanocrystals and deposition of such dispersion results in preferential anchoring of Au nanocrystals onto thiol-patterned surface [109]. However, this type of assembling is applicable only to specific binding combination. A more generic method is making using of the wettability of the template surface. The substrate surface is patterned with hydrophobic and hydrophilic regions (Fig. 2.3d–g). Any 1D nanocrystals that are dispersed in the water are able to remain in the hydrophilic patterns when the excess suspension is withdrawn by pipette. Once the water is evaporated, the 1D nanocrystals are confined within the designed hydrophilic regions [113]. The orientation of 1D nanocrystals inside the hydrophilic regions can be further controlled by narrowing the width of hydrophilic region. When the width of hydrophilic region is less than the length of nanorods or nanowires, these nanocrystals align along the longitudinal axis of hydrophilic region.

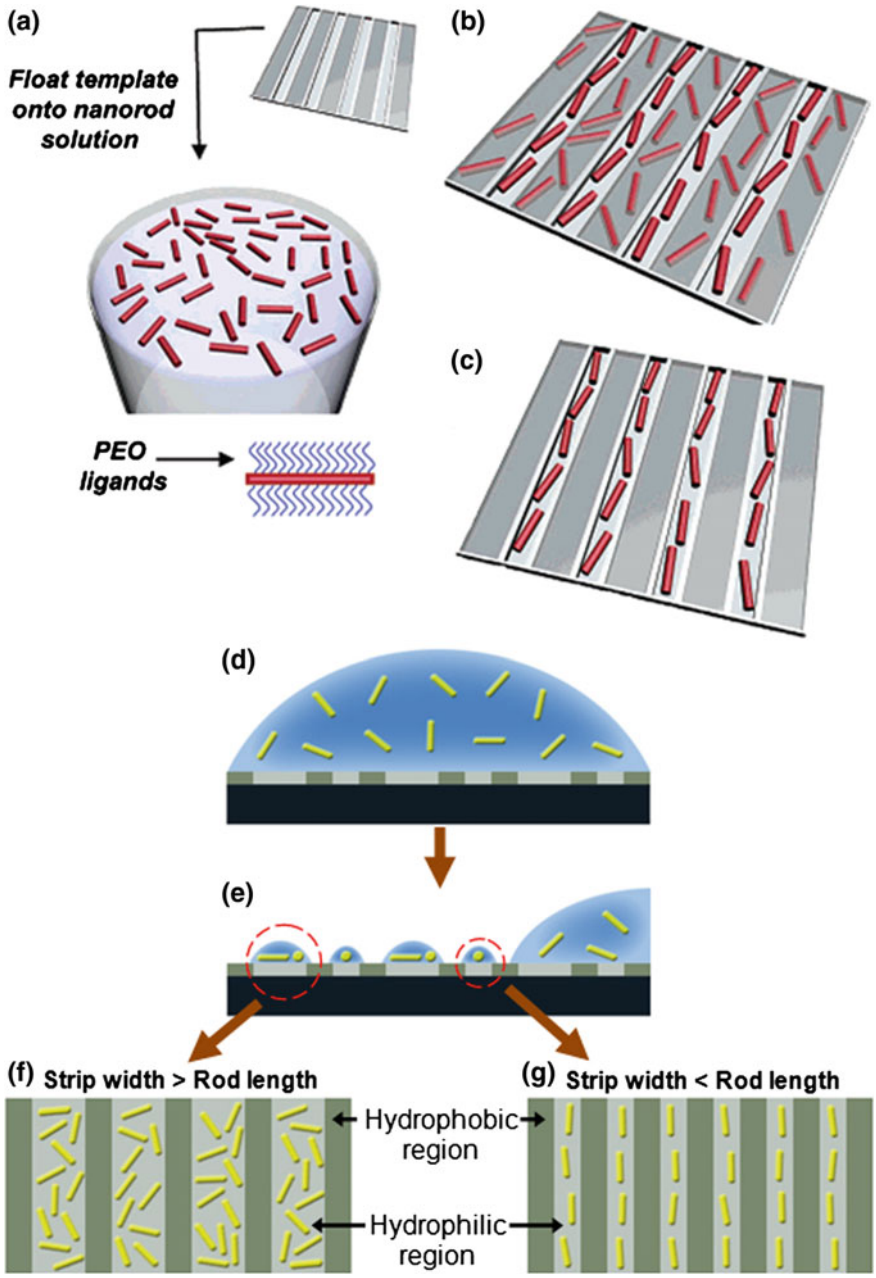
(a)
Float template onto nanorod solution
PEO ligands
(b)
(c)
(d)
(e)
(f) Strip width > Rod length
(g) Strip width < Rod length
Hydrophobic region
Hydrophilic region

◀ **Fig. 2.3** Template-assisted assembly. **a–c** Schematics of template-assisted assembly process via geometric confinement: **a** flotation of template onto aqueous solution of PEO-covered CdSe nanorods; **b** CdSe nanorods within the channels and on the template surface; **c** CdSe nanorods isolated in the channels following rinsing of the template. Reproduced with permission from [114]. **d–g** Schematics of template-assisted assembly process via chemical interaction: **d** a nanowire suspension is drop-casted on substrates with hydrophilic and hydrophobic patterns; **e** settling of nanowires onto substrates; **f** formation of discrete droplets during the removal of the nanowire suspension; **g** patterned nanowires on substrates. Reproduced with permission from [113]

2.2.2 Self-assembly at Interfaces

Self-assembly at the interface has been observed and studied for more than a century. A well-known example is Pickering emulsions, in which solid particles adsorb at the paraffin-water interface to stabilize the emulsion droplets from coalescence [129, 130]. This phenomenon has been extended to self-assemble colloidal micron-sized particles and later on nanocrystals between two immiscible phases. The alignment of particles at the interface can cause a reduction of total interfacial energy and it is the dominant force in driving such self-assembly. If the decrease of the interfacial energy is larger than the thermal energy that causes fluctuations, the colloidal particles can be aligned at the interface. In general, the interfacial energy is related to the particle size by Pieranski's theoretical calculation [131–134]. The total decrease of interfacial energy is smaller for small particles and therefore, interfacial assembly originally only targets micro-sized particles. Nevertheless, recent studies have successfully demonstrated 1D nanocrystals self-assembly at interface, offering a flexible pathway for bottom-up assembly of nanorods or nanowires into organized structures [135–138].

The Langmuir-Blodgett (LB) and Langmuir-Schaefer (LS) techniques are the most widely used and developed methods in achieving 1D nanocrystal assembly at interface. The nanorods or nanowires are required to be protected with hydrophobic capping ligands [54] and spread evenly on the water surface. At the air-water interface, the randomly orientated nanocrystals are compressed slowly using a barrier with the surface pressure monitored (Fig. 2.4a–c). At different stages of compression, a horizontally aligned monolayer or nematic, smectic aligned multilayer nanocrystals assemblies can be observed and collected onto desirable substrate using either vertical (LB technique) or horizontal (LS technique) deposition procedure [62]. The assembled 1D nanocrystals exhibit remarkable alignment parallel to the barrier. Providing suitable surface passivation chemistry, this interface-based method is applicable to various 1D building blocks, and the assembled structure size, packing order and inter-nanocrystal spacing can be controlled independently with engineering precision [135].

Deposition at the oil/water interface is another extensively studied technique in directing self-assembly of 1D nanocrystals. The purified 1D nanocrystals are first dispersed in organic solvent that is immiscible with water and has a low vapor pressure. A small amount of such dispersion is drop-casted carefully onto the water

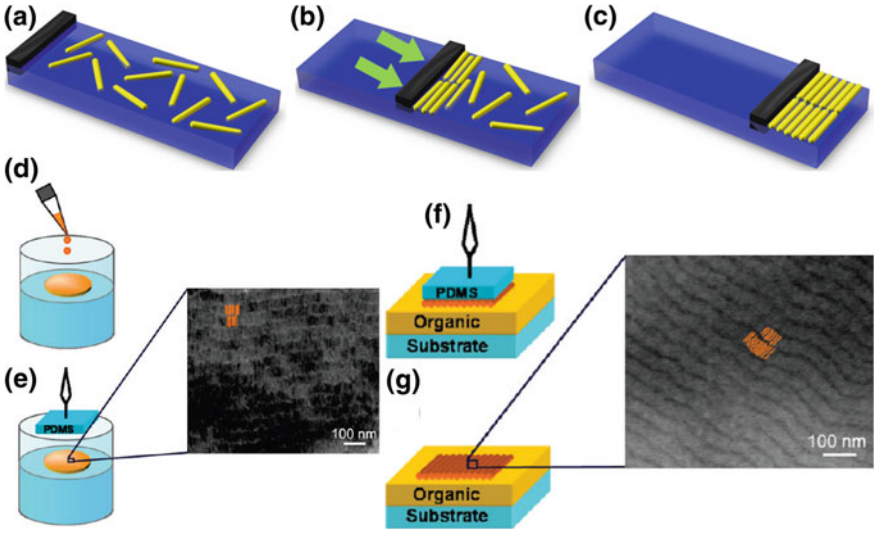

Fig. 2.4 Self-assembly at interfaces. **a–c** Schematics of Langmuir-Blodgett nanorod assembly at the air-water interface. **a** Random distribution of nanorods at air-water interface. **b** Organization of nanorods as the barrier compressing the nanorods. **c** Assembled structures when barrier reaches final compression stage. **d–g** Schematics of nanorod assembly at water-toluene interface. **d** CdSe/CdS nanorods in toluene are spread dropwise on water surface. **e** After the toluene evaporation, the floating film is harvested by liftoff of a PDMS stamp pad. The zoomed image shows a TEM image of self-assembled CdSe/CdS nanorods. **f** The inked PDMS is brought into contact with the organic layer by a gentle pressure. **g** The self-assembled is transferred onto organic surface after PDMS stamp is removed. The zoomed image shows a SEM image of self-assembled CdSe/CdS nanorods. Reproduced with permission from [49]

surface. The 1D nanocrystals are able to aggregate and align at the oil/water interface while the organic solvent is allowed to evaporate slowly over a period of several hours (Fig. 2.4d–g). The in-plane compression, interfacial tension and the capillary force mediate the assembly of 1D nanocrystals. The ordered structures are then harvested by a contact printing technique with a hydrophobic substrate, e.g. polydimethylsiloxane (PDMS) stamp pad and eventually transfer to a device [49]. These individual 1D nanocrystals assembled at the interface maximize the interfacial coverage per nanocrystal and minimize the Helmholtz free energy of the whole system. Due to its anisotropic nature, the 1D nanocrystals aligned parallel to the interface generally cover more surface area and possess much lower interfacial energy than those oriented perpendicular to the interface [132]. However, the nanorods orientated perpendicular to the interface are still observed when the concentration of nanorods reach a critical value [30, 133]. The interfacial energy between liquids and nanocrystals, the aspect ratio and concentration are the major parameters in controlling the orientation and structures of 1D nanocrystals interfacial assembly.

2.2.3 Self-assembly in Solutions

Solution based assembly is perhaps the most simple while complicated method in achieving 1D nanocrystals self-assembly. It is simple as it involves little or no external facilitations (e.g. electric-filed, template), while enables the nanorods or nanowires spontaneously assembled within the solution [58, 137, 139–143]. It is complicated as it engages a variety of chemical interactions, e.g. hydrogen bond, chemical bonding, electrostatic force [144–151], among the whole spectrum of nano-entities inside the solution. Each of the interaction works in a unique way and is very specific towards different combinations of nanocrystals, capping ligands and solvent. In that sense, the solution-based assembly is a complicated method requires dedicated design of the whole solution system.

Although the driving forces vary for different solution based assemblies, this type of assemblies, however, shares a similar process. At first glance, small self-assemblies are formed randomly in the solution due to the chemical interactions and collisions caused by the Brownian motion. These small self-assemblies, serve as nucleation sites, subsequently draw neighboring building blocks together and grow into ordered microscale structures [152–155]. The assembly process is closely related to the concentration and temperature of the stocking solution. In general, as the concentration of 1D nanocrystals and temperature increase, the collisions between the nanocrystals are more frequent and thus the assembling of collided nanocrystals become easier and faster [156]. A selective change of solvent quality can trigger or facilitate the above process, by causing the destabilization of a well-dispersed nanocrystal solution [74, 138, 155, 157].

Making use of the hydrogen bond of capping ligand is one frequently used method in directing solution-based assembly. Bifunctional molecules such as cysteine, glutathione, 3-mercaptopropionic acid, 11-mercaptoundecanoic acid, and α,ω-alkanedithiols which carries thiol group are shown selectively bind to the end or side surface of Au nanorods via hydrogen bonds [145, 148, 156–158]. This hydrogen bonding can be controlled by the variation of the pH value of the solution, which enables the Au nanorods assembled in a side-by-side (Fig. 2.5a) or end-to-end (Fig. 2.5b) pattern or disassembled back to random alignment. The pH value of solvent close to these bifunctional molecules PK_a value favors the assembly while the pH value away from the PK_a value favors the disassembly, which agrees with the hydrogen-bonding theory. Other than hydrogen bond between the capping ligands, the chemical bonding is another useful force in assembling 1D nanocrystals. Zhang et al. have reported chemical bond driven self-assembly of CoP nanowires when aging them in the reaction solution for 120 min [159]. The capping ligands adsorbed/desorbed from CoP nanowires dynamically in the mother reaction solution, and their controlled removal led to direct interaction between adjacent nanowires to form Co-P chemical binding. As shown in Fig. 2.6a, b, this chemical bond was direction-specific, forcing nanowires position in a particular facet, thus

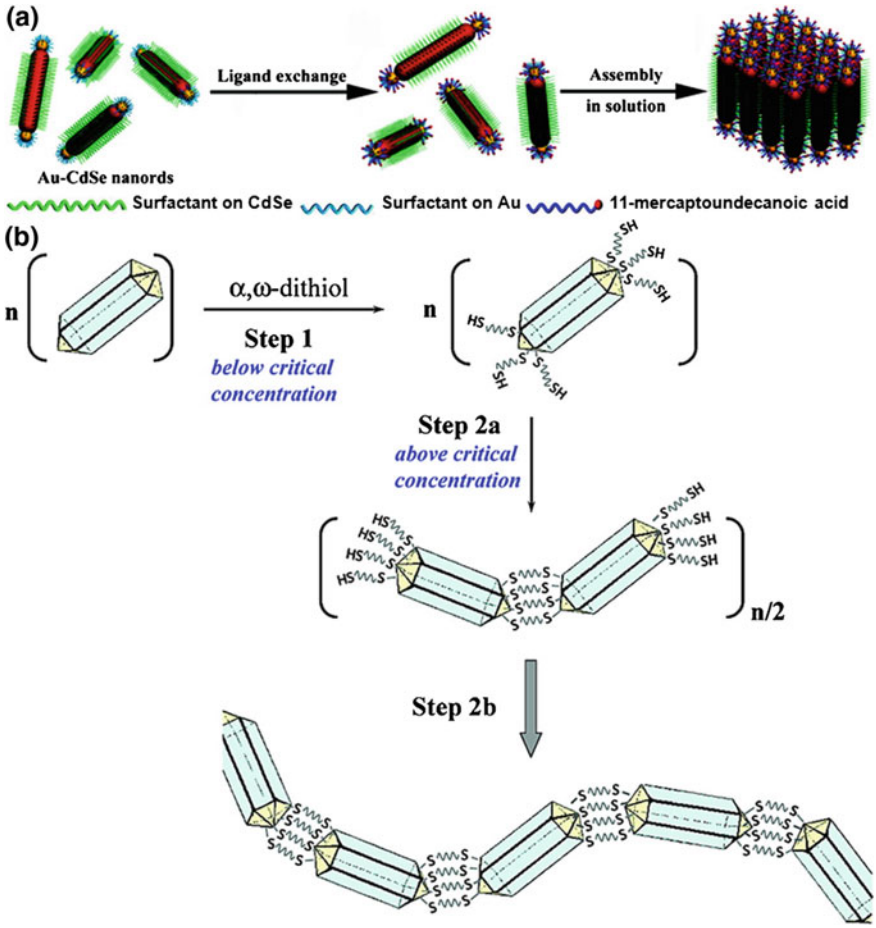

Fig. 2.5 Self-assembly in solutions. **a** Schematics of the side-by-side self-assembly of Au-tipped CdSe nanorods via hydrogen bonds. The Au tips are ligand-exchanged with 11-mercaptoundecanoic acid and cross-linked via hydrogen bonds between their carboxylic groups. Reproduced with permission from [157]. **b** Schematics of the end-to-end self-assembly of Au nanorods via hydrogen bonds. (Step 1) The Au tips are capped with α,ω-alkanedithiols. (Step 2a) Above a critical concentration of α,ω-alkanedithiols, nanorods form dimmers and (Step 2b) subsequently chain structure via hydrogen bonds between their thiol groups. Reproduced with permission from [148]

provided both positional and orientational order. In addition, electrostatic force [160], depletion attraction (Fig. 2.6c–f) [161] and avidin-biotin recognition [144, 162] have also been demonstrated successfully in self-assembling nanorods or nanowires at specific locations to form ordered close-packed or non-close-packed structures.

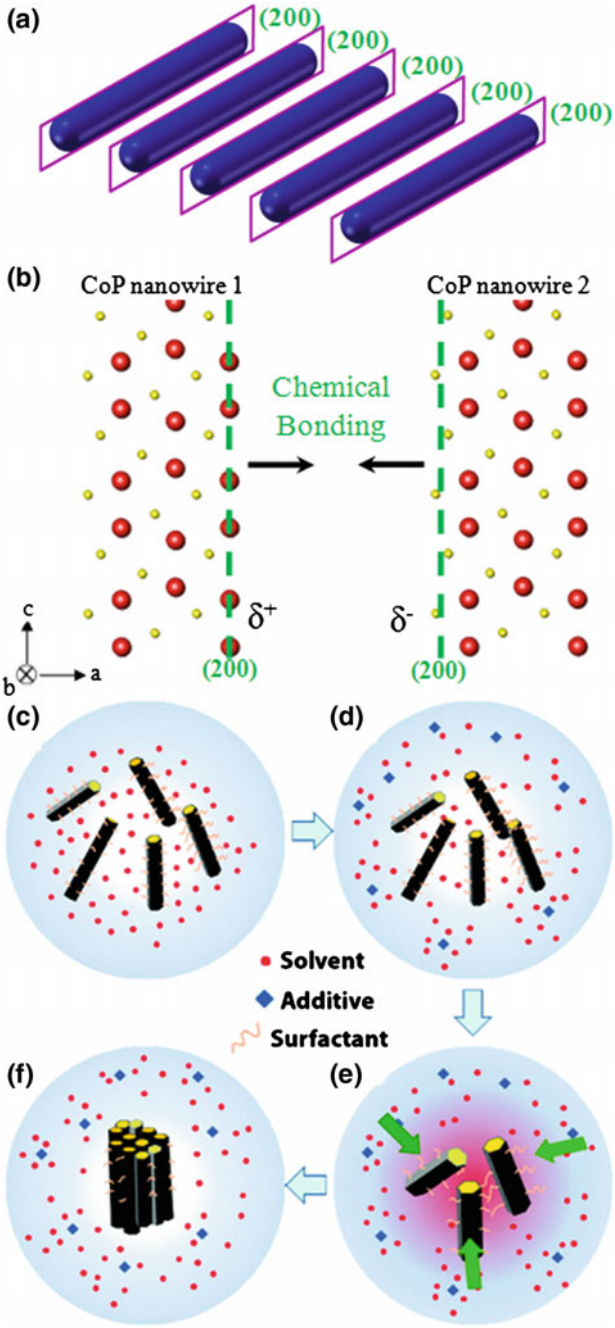
(a)
(200)
(200)
(200)
(200)
(200)
(b)
CoP nanowire 1
CoP nanowire 2
Chemical
Bonding
δ+
δ-
(200)
(200)
c
b
a
(c)
(d)
Solvent
Additive
Surfactant
(f)
(e)

◀ **Fig. 2.6** Self-assembly in solutions. **a–b** Schematics of solution-based self-assembly of CoP nanowires via chemical bonds. **a** The CoP nanowires are aligned along (200) facet and **b** allow the irreversible formation of chemical bonds between Co and P atoms from neighboring nanowires. Reproduced with permission from [159]. **c–f** Schematics of solution-based self-assembly of CdS, CdSe, CdS/CdSe nanorods via depletion attraction. **c** Nanorods coated with hydrophobic surfactant are dispersed in organic solvent. **d** Assembly is triggered by introducing additive (macromolecule) into the solvent. **e** An osmotic pressure (depletion attraction) is developed and drive nanorods aligned together when nanorods approach each other and create a volume inaccessible to additive. **f** Final assembled structures. Reproduced with permission from [161]

2.3 Self-assembly Packing Structures

Other than various methods that have been demonstrated to self-assemble 1D nanocrystals, numerous packing orders have also been achieved using these 1D building blocks. Different from the *fcc* or *hcp* pattern that is typically formed by isotropic nanocrystals, the anisotropic nature of 1D nanocrystals renders them great possibility to be arranged into diverse packing orders, such as stripes, horizontal/vertical monolayer, nematic/smectic multilayer, AB stacking of vertical alignments, and 3D assemblies. The assembled structures from 1D nanocrystals usually possess both positional and orientational orders that require precise alignment of building blocks. The collective properties of these assembled structures differ from their individual building blocks and vary upon the change of the packing order. In this section, we review various alignments that have been achieved in self-assembling 1D nanocrystals with the emphasis on the nanorod and nanowire building blocks.

2.3.1 Non-close-Packed Structures

The non-close-packed structures formed by the 1D nanocrystals refer to the self-assembled structures that are not continuously aligned over a large-scale area in at least two directions, e.g. x, y directions in Cartesian coordinates. They are of low surface coverage and generally in the form of networks of stripes pattern (also called ribbons or chains in some literatures) with substantial amount of space in between [163–165]. Each stripe is a single layer structure, which can reach several micrometers long. These stripes are usually placed independently with low level of ordering (Fig. 2.7a–d). However, within the stripes, the building blocks are well organized in two basic alignments: side-by-side or end-to-end. A single stripe pattern can consist of either one of these alignments or a combination of both. In general, the inter-nanorod/nanowire energetic forces such as van der Waals force, dipole-dipole interaction favor side-by-side alignment due to the large contact area when they are aligned along the longitudinal axis. This alignment is widely observed in various stripe patterns. Nevertheless, in certain cases, such as a kinetically limited self-assembly process [166], end-to-end structures can be the dominated form in composing the stripes.

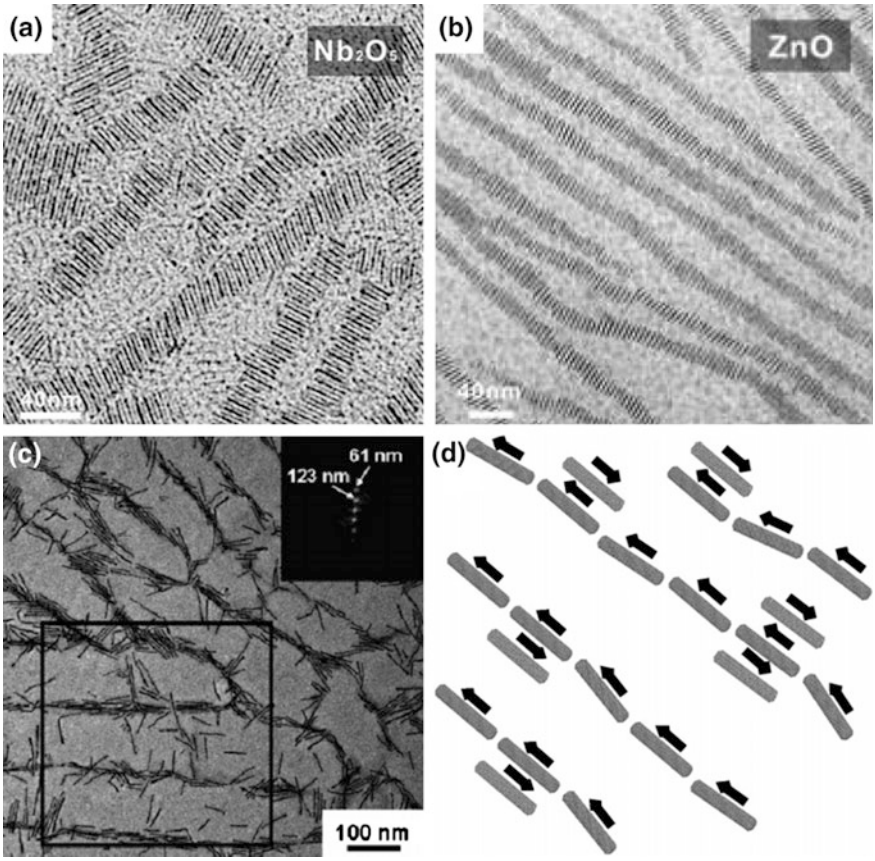

Fig. 2.7 TEM images of side-by-side stripe pattern formed by **a** Nb_2O_5 nanorods, **b** ZnO nanorods. Reproduced with permission from [143]. **c** TEM images of primarily end-to-end stripe pattern formed by CdS nanorods. The *inset* shows an FFT of the region enclosed by an outlined square. **d** Corresponding schematic diagram of primarily end-to-end stripe pattern. Within the stripes, a few nanorods are packed side-by-side, an orientation favored by both antiparallel dipole interactions (represented by the *black arrows*) and van der Waals attraction. Reproduced with permission from [166]

One example of non-close-packed structures that are based on side-by-side alignment is displayed in Fig. 2.7a, b, which has been reported by Yang and his co-workers [143]. Nb_2O_5 nanorods with diameter of 1.3–1.6 nm (Fig. 2.7a) and ZnO nanorods with diameter of 1.1–1.4 nm (Fig. 2.7b) were demonstrated to be self-assembled into well-defined, uniform, stripe structures that could reach 1.6 μm in the length with aspect ratio of ~ 80. The side-by-side arrangements here created the largest contact area for the neighboring nanorods, and thus ensured the formation of stripes through the interactions between surfactants and inorganic species. A range of sub-2 nm (down to one unit cell) transition metal oxide (TiO_2,) and rare earth

oxides (Eu_2O_3, Sm_2O_3, Er_2O_3, Y_2O_3, Tb_2O_3, and Yb_2O_3) were also demonstrated to be self-assembled into arrays of stripes.

The end-to-end alignment in the non-close-packed structures is mostly seen when specific bindings, e.g. hydrogen bonding, exist at the tips of the nanorods/nanowires, as the case we mentioned in solution based assembly (Fig. 2.5b). The contact area of end-to-end alignment is much limited compared with side-by-side configuration, and therefore it is not the preferred structures. Nevertheless, Korgel and his co-workers showed in a kinetically limited self-assembly process, in which the CdS nanorods formed primarily end-to-end alignments (Fig. 2.7c) when evaporating a small amount of CdS colloidal solution at a low surface coverage. The evaporation process promoted a kinetically limited structure (Fig. 2.7d) via the spinodal decomposition. There was also a preferred orientation of the stripes as shown by the fast Fourier transforms (FFT) image in Fig. 2.7c inset. The distances specified by the linear spot positions in FFT corresponded to the distances between stripes (center to center). However, when the FFT was taken at a large scale of multiple domains of stripes, a diffuse ring instead of spots was observed, suggesting the stripe pattern lacked long-range ordering [166].

The non-close-packed structures can also be constructed from a combination of both side-by-side and end-to-end alignments. Each stripe pattern, for instance, is able to consist of a few columns of nanorods that are aligned end-to-end. Meanwhile, within each column, the nanorods are attached to each other via a side-by-side alignment. Such structures require dedicated constrains in directing nanocrystal alignment, and are usually achieved with the aid of external facilitation. The internal organization of stripes such as the number of columns in a single stripe can be further controlled by adjusting external facilitation. The competition between the side-by-side and end-to-end alignments within the stripes is a destabilizing factor that can lead to the disorganization of the self-assembly. Banin and his colleagues have used a copolymer film as a template, to successfully self-assemble polystyrene-coated (PS-coated) CdSe nanorods into non-close-packed structures with both side-by-side and end-to-end alignments (Fig. 2.8a–d) [125]. The copolymer film was casted from polystyrene-block-poly(methyl methacrylate) (PS-b-PMMA) and featured with alternating PS and PMMA domains. The PS-coated CdSe nanorods were therefore selectively bound to the PS domains on the template. By aligning perpendicular with respect to their hosting PS domains, the CdSe nanorods maximized attractive van der Waals interactions from neighboring nanorods, while minimized the repulsive interactions from surrounding PMMA domains (Fig. 2.8b). Via adjusting the ratio between the PS domain width and the nanorod length, the CdSe could form multiple end-to-end aligned rows. However, this orientational preference of nanorods in both side-by-side and end-to-end alignment diminished for decreasing nanorod aspect ratio and gave way for adverse orientational entropy effects [126]. The long nanorods with long copolymers template were preferred for highly organized stripe patterns as short nanorods and/or short copolymers were more prone to morphological defects.

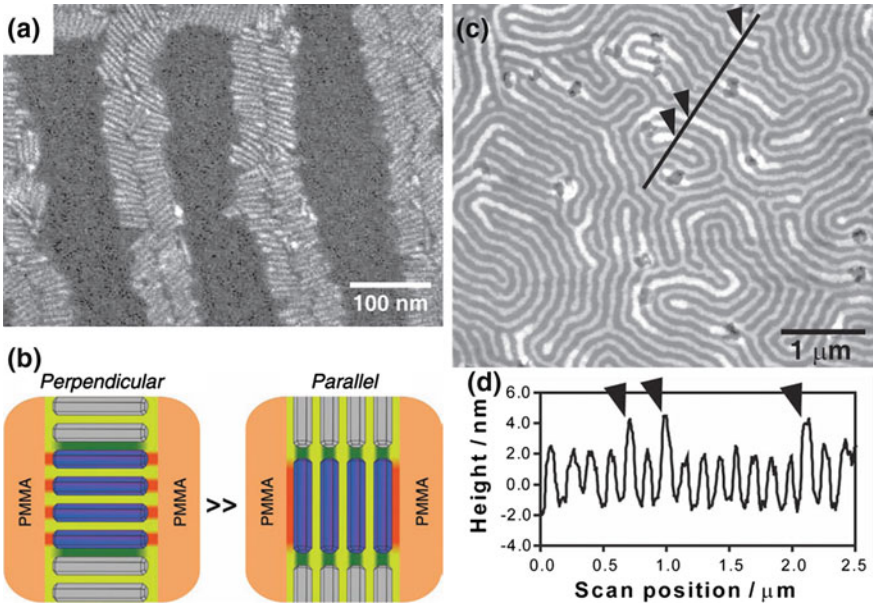

Fig. 2.8 **a** SEM images of non-close-packed structures formed by PS-coated CdSe nanorods on PS-*b*-PMMA coated substrate, showing a coexistence of both side-by-side and end-to-end alignments. **b** Schematic diagram showing the preferential alignment of the perpendicular orientation over the parallel orientation with respect to their hosting PS domain. The attractive and repulsive interactions depicted as *green* and *red* stripes, respectively; while PMMA domains are colored *orange*, and PS domains underneath the nanorods are colored *yellow*. **c** AFM micrograph of non-close-packed structures formed by PS-protected CdSe nanorods on PS-*b*-PMMA coated substrate. *Height scale* 10 nm. **d** AFM height profile corresponds to the *black line*, where *arrowheads* mark crossed nanorod-filled PS domains. Reproduced with permission from [125]

2.3.2 Close-Packed Monolayers

2.3.2.1 Horizontal Alignment

Close-packed monolayers in horizontal alignment from 1D nanocrystals are simple two-dimentional (2D) planar monolayer structures, with all building blocks closely assembled and arranged horizontally with respect to the monolayers. In an ideal scenario, the longitudinal axes of these building blocks are aligned parallel to one common direction to maximize the attractive interactions while maintain the lowest system energy. One typical example of such parallel structures is the Langmuir-Blodgett film (Fig. 2.4a–c); in which all 1D nanocrystals' longitudinal axes are aligned parallel to the barrier when the barrier compresses the air-water interface slowly. The alignment along the 1D nanocrystals' transverse direction, however, enjoys more degrees of freedom. As shown in Fig. 2.9a, the ZnS nanorods in the transverse direction form zigzag staggered rows with neighboring nanorods

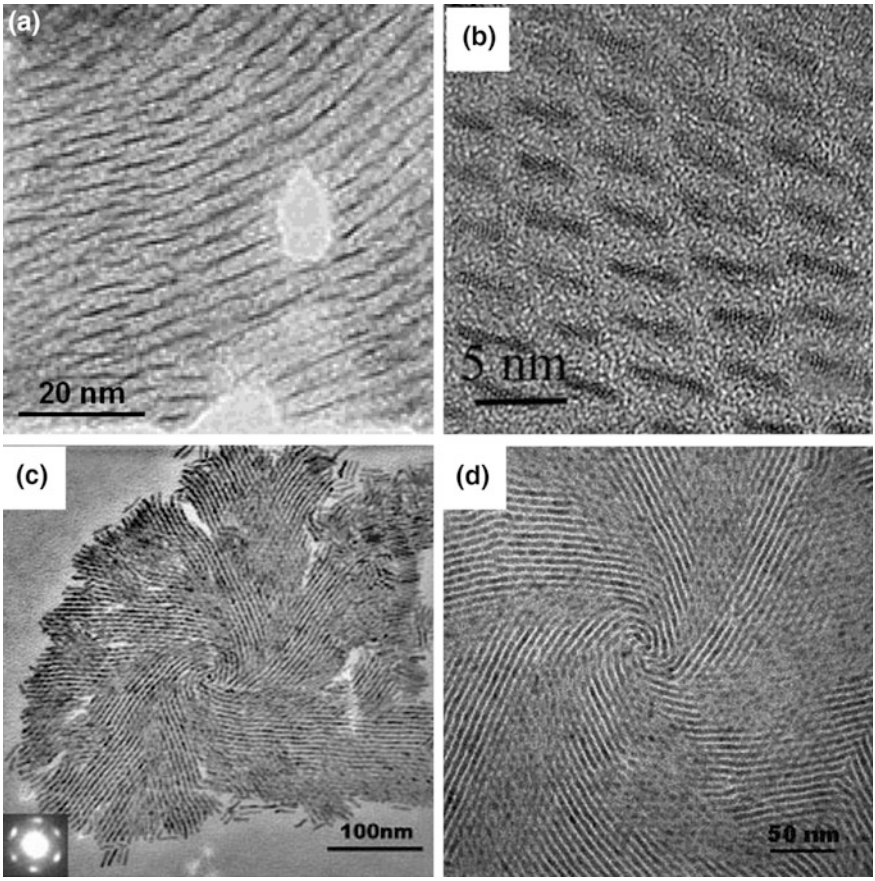

Fig. 2.9 TEM images of horizontally aligned ZnS nanorod monolayer in **a** zigzag staggered structures and **b** layered structures. Reproduced with permission from [137]. **c** TEM and **d** magnified TEM images of horizontally aligned CdSe nanorod monolayer in disclination structures. The *inset* of **c** gives the corresponding SAED pattern. The disclination structure nucleates at the *center* and grows into six branches with angel discontinuity of 60°. Reproduced with permission from [139]

overlapping with each other. This arrangement is sometimes termed as 2D nematic phase (see nematic alignment in 2.3.3 close-packed multilayers for more details). In addition to the zigzag-staggered structures, 1D nanocrystals in the transverse direction can also form ordered rows without overlapping. Showing in Fig. 2.9b, the ends of any ZnS nanorod are evenly spaced with the ends of other nanorods either ahead or behind it [137]. This forms layered structures in the transverse direction and is sometimes termed as 2D smectic phase (see smectic alignment in 2.3.3 close-packed multilayers for more details).

Other than longitudinal axes aligned parallel to one common direction, the self-assembly of 1D nanocrystals in the horizontal alignment can exhibit a disclination structure. It is usually observed as a disruption towards the long-range parallel structures, where the director of individual nanorods/nanowires changes continuously about the center [135]. The disclination structure is initially thought energetically unfavorable and should not occur for the monolayer system. However, Alivisatos's group [139] later observed a disclination structure in a vortex shape with CdSe nanorods. Figure 2.9c showed an isolated vortex-shaped self-assembly, the inset of which gave the corresponding selected area electron diffraction (SAED). The hexagonal spot pattern from SAED indicated a sixfold symmetry of ordering. A magnified image in Fig. 2.9d further revealed CdSe nanorods around the center were separated into six branched, which agreed with SAED pattern. Within each branch, the nanorods were arranged parallel to a common direction and formed a distinct crystalline domain. In-between two adjacent branches, a discontinuity of 60° in nanorod orientation existed. The centers of disclination structures were generally regarded as defects, which served as nucleation sites for the disclination structure to grow.

In the horizontal alignment, the inter-nanocrystal spacing is an important parameter that influences the collective property of the whole assembly. It is shown this spacing affects the coupling between adjacent nanocrystals and therefore coupled plasmon modes that give rise to coherent propagation of energy along the array. When the spacing is well adjusted, the assembled monolayer is able to propagate light along the nanorod–nanorod chain effectively [52, 167]. In general, the inter-nanocrystal spacing remains the same within one horizontally aligned monolayer, even for the 1D nanocrystals aligned differently at the ends. As illustrated in Fig. 2.10a, b [58, 142], two ends of neighboring Au nanorods were either aligned perfectly along the same axis (eclipsed end-to-end, Fig. 2.10a), or had a lateral displacement (staggered end-to-end, Fig. 2.10b). Though these two arrangements were different in organizing the structure, the inter-nanorods spacing between two ends of the Au nanorods were shown to be the same, $\sim$8.5 nm. This spacing also coincided with the distance between two sides of neighboring Au nanorods. The inter-nanocrystal spacing generally remains constant for the same monolayer, but varies for different monolayers. In the case of Langmuir-Blodgett film, the inter-nanocrystal spacing can even be manually controlled through the compression pressure.

Unlike the self-assembly structures from spherical nanocrystals, some horizontally aligned monolayers have exhibited both positional and orientational orders due to their anisotropic building blocks. Zhang et al. have reported a solution-based self-assembly process in which horizontally aligned CoP nanowire monolayers were assembled with the same facet orientation. The CoP nanowires with aspect ratio greater than 40 were self-assembled into monolayers with horizontal alignment. As shown in the Fig. 2.10c, the CoP nanowires were aligned along their longitudinal axes and close-packed with neighboring nanowires. The corresponding FFT in Fig. 2.10d clearly indicated a linear spot diffraction pattern that signified the parallel alignment and same inter-nanowire distance (center to center).

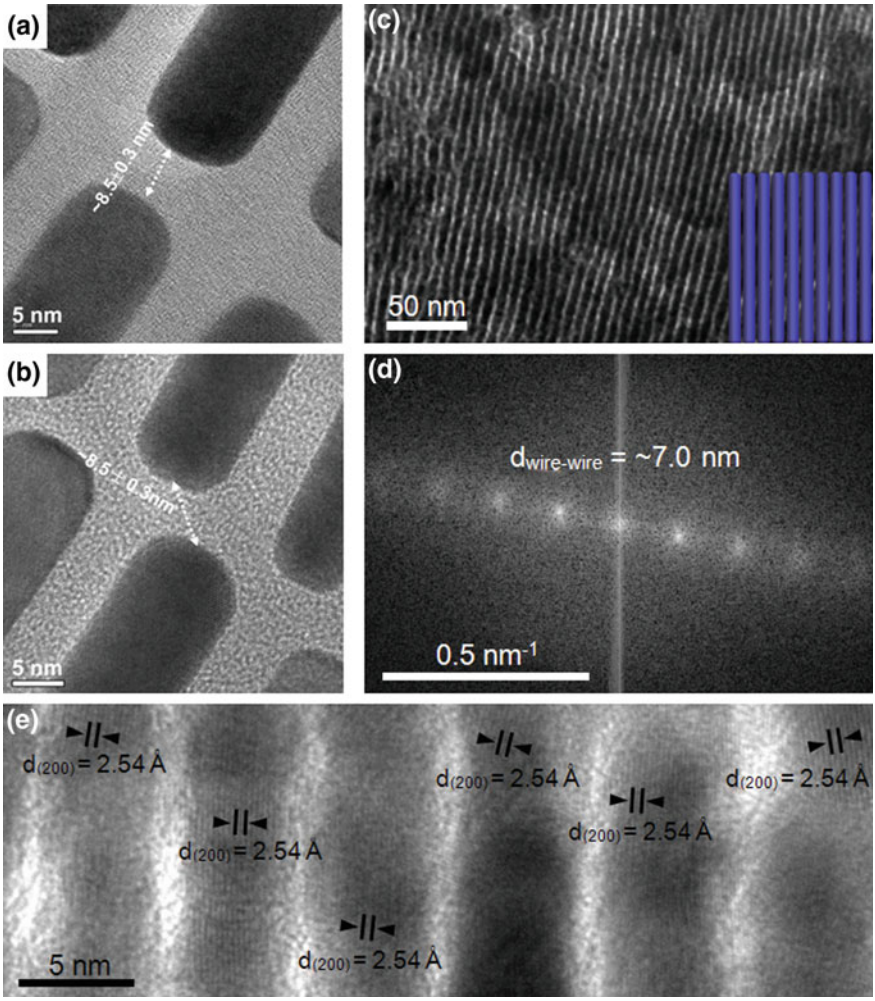

Fig. 2.10 TEM images of horizontally aligned Au nanorod monolayer in **a** eclipsed end-to-end and **b** staggered end-to-end patterns. Reproduced with permission from [142]. **c** TEM and **d** corresponding FFT images of horizontally aligned CoP nanowire monolayer. **e** HRTEM images of six neighboring CoP nanowires, showing uniform lattice orientation from (200) planes. Reproduced with permission from [159]

The HRTEM image revealed that all the (200) planes were parallel in the adjacent CoP nanowires, indicating the oriented attachment of nanowires with the same lattice orientation. This orientational order is particular important for the anisotropic materials, as the collective properties are associated with their anisotropy, e.g. magnetism, can be maintained and even strengthened.

2.3.2.2 Vertical Alignment

Close-packed monolayers in vertical alignment from 1D nanocrystals are three-dimentional (3D) block monolayer structures, with all building blocks closely assembled and arranged vertically with respect to the monolayers. Vertical alignment of nanorods is of special interest because it helps to further minimize the size below the lithographic limit and exhibit single transistor behavior [168]. For a vertically aligned monolayer that perfectly aligned, it possesses a honeycomb structure, as the case in Fig. 2.11a, b. When viewing from top of such monolayer, (Fig. 2.11a), each of the 1D nanocrystals stands perpendicularly to the substrate and is surrounded by six neighboring nanocrystals. These six nanocrystals form a hexagonal pattern, which achieves the highest packing efficiency that is energetically favorable. The lateral arrangement of neighboring nanocrystals is similar to those in horizontally aligned monolayers (Fig. 2.11b), in which the longitudinal axes of these 1D building blocks are aligned parallel to one direction so as to maximize the attractive interactions [157].

Similarly to the horizontally aligned monolayers, some vertically aligned monolayers also possess both positional and orientational orders. Ryan's group [75] has observed the anisotropic CdS nanorods were aligned vertically in the hexagonal shape on a substrate with uniform lattice orientation (Fig. 2.11c–e). The transmission electron diffraction pattern of a single crystal (Fig. 2.11d) revealed its perfect wurtzite crystal structure from [001] zone axis. Close analysis from the HRTEM image in Fig. 2.11e indicated clearly a similar orientation of (100) planes from the vertically aligned nanorods. Only a slight angular variation of ±6 °C was observed for (100) planes from neighboring nanorods that affirmed the orientational ordering. A quantitative assessment of vertically aligned nanocrystals can be further calculated based on the building blocks' orientational ordering. Since the nanocrystals are assembled with uniform lattice orientation, the information of the lattice orientation can be transferred into the information of the nanocrystal orientation. Alivisatos's group has demonstrated an evaluation technique in assessing the percentage of vertically aligned CdS nanorods against entire nanorod population using grazing-incidence wide-angle X-ray diffraction. The longitudinal axes of these wurtzite CdS nanorods coincided with the *c*-axis [001] direction. When the nanorods were aligned vertically as shown in Fig. 2.11f, the diffraction pattern from (002) planes (blue dashed line in Fig. 2.11g) reflected to the top of Bragg ring, which corresponded to the ω direction at 0° (green arrow in Fig. 2.11g). Integrating diffraction intensity of (002) planes as a function of ω gave the orientation distribution, with the ω = 0° refer to the vertically aligned structures. In the case they demonstrated, 75 % nanorods were self-assembled in the vertical alignment [93].

As the vertical and horizontal alignment share similar structure properties, experiment has shown the coexistence of horizontally and vertically aligned structures [30, 169]. A concentration correlation with the packing order has been observed when drying colloidal water droplets containing CdSe nanorods [100, 133]. At a high concentration region (e.g. the center of the droplet), the nanorods are aligned vertically to the substrate. However, at a low concentration

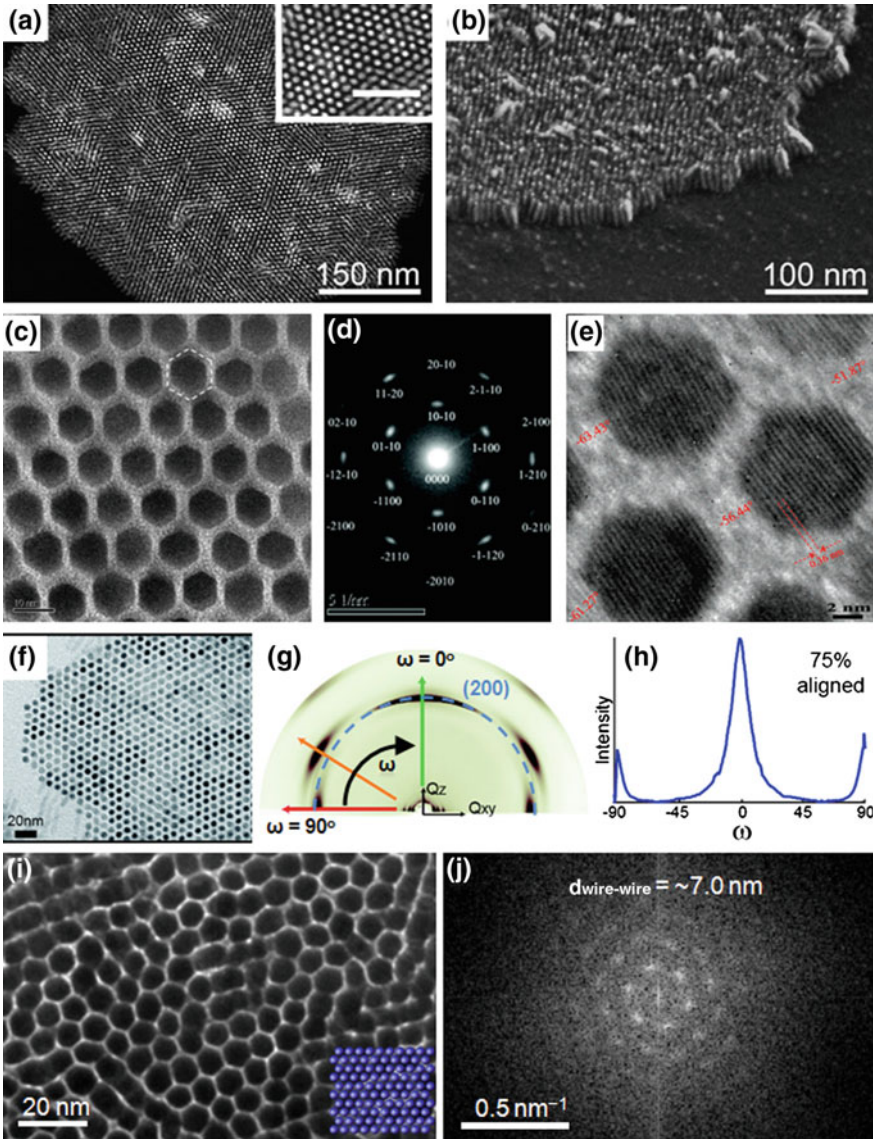

region (e.g. in between the center and periphery of the droplet), the nanorods are aligned horizontally to the substrate. At the lowest concentration region (e.g. the periphery of the droplet), a less-organized structure with nanorods in local ordering is observed. In addition to the coexistence of horizontally and vertically aligned structure, Zhang et al. have demonstrated a selective alignment at different aging temperature. For example, at low aging temperature 0 °C, the CoP nanowires were found to form horizontally aligned monolayers (Fig. 2.10c). While at high aging

◀ **Fig. 2.11** **a** *Dark* field TEM image (*top view*) and **b** SEM image (*side view*) of vertically aligned Au-tipped CdSe nanorod monolayer. The *inset* of **a** shows a magnified image and the *scale bar* represents 50 nm. Reproduced with permission from [157]. **c** TEM image of vertically aligned CdS nanorod monolayer. **d** Single-crystal electron diffraction indexing of one CdS nanorod at [001] zone axis. **e** HRTEM image of three neighboring CdS nanorods, showing uniform lattice orientation from (100) planes. Reproduced with permission from [75]. **f** TEM image and **g** X-ray diffraction pattern of vertically aligned CdS nanorod monolayer. The diffraction from (200) planes is marked by *blue dashed line*. The *green arrow* at ω = 0° corresponds to vertically aligned nanorods; the *red arrow* at ω = 0° corresponds to horizontally aligned nanorods. **h** Orientation distribution of vertically aligned CdS nanorods obtained by plotting the diffraction intensity of (002) planes in **g** as a function of ω. Reproduced with permission from [93]. **i** TEM and **j** corresponding FFT images of vertically aligned CoP nanowire monolayer. Reproduced with permission from [159]

temperature, *i.e.* room temperature, the CoP nanowires formed vertically aligned monolayers (Fig. 2.11i). The inter-nanowire distance (center to center) given by the FFT image (Fig. 2.11j) is ~7.0 nm, which was the same as the spacing in the horizontal alignment, suggesting the basic unit of horizontal and vertical alignment was similar.

2.3.3 Close-Packed Multilayers

2.3.3.1 Nematic Alignment

"Nematic" is a common term used primarily in describing the phase of liquid crystals. It refers to the organization of liquid molecules with a long-range orientational order in the longitudinal direction but no translational order. The liquid molecules in nematic liquid crystals are free to flow and randomly distributed as long as they keep the orientational order. Some of close-packed multilayer structures self-assembled from 1D building blocks resemble this ordering; and the term "nematic" has been borrowed to describe such structures. As shown by the SEM image in Fig. 2.12a, a nematic aligned multilayer structure has all longitudinal axes of Au nanorods pointing in the same direction. However, in the transverse direction, there is no periodicity observed for the Au nanorods. The FFT pattern of nematic alignment (Fig. 2.12a inset) also reveals single-direction diffuse streaks, which agrees with the long-range orientational order but no translation order. The nematic alignment can be viewed as the 3D assembly of nanocrystals in two steps. The nanorods/nanowires are first assembled together in an end-to-end pattern to form stripes (chains). These stripes are then packed together, nearly parallel to each other, into a 3D structure [94].

Similar to the liquid crystals, the nematic alignment of 1D nanocrystals is frequently observed in the electric-field-assisted assembly. The anisotropic 1D nanocrystals, especially metal, oxide, sulfide, can be polarized and behave like liquid crystals in the electric filed. When an external electric field is applied to the

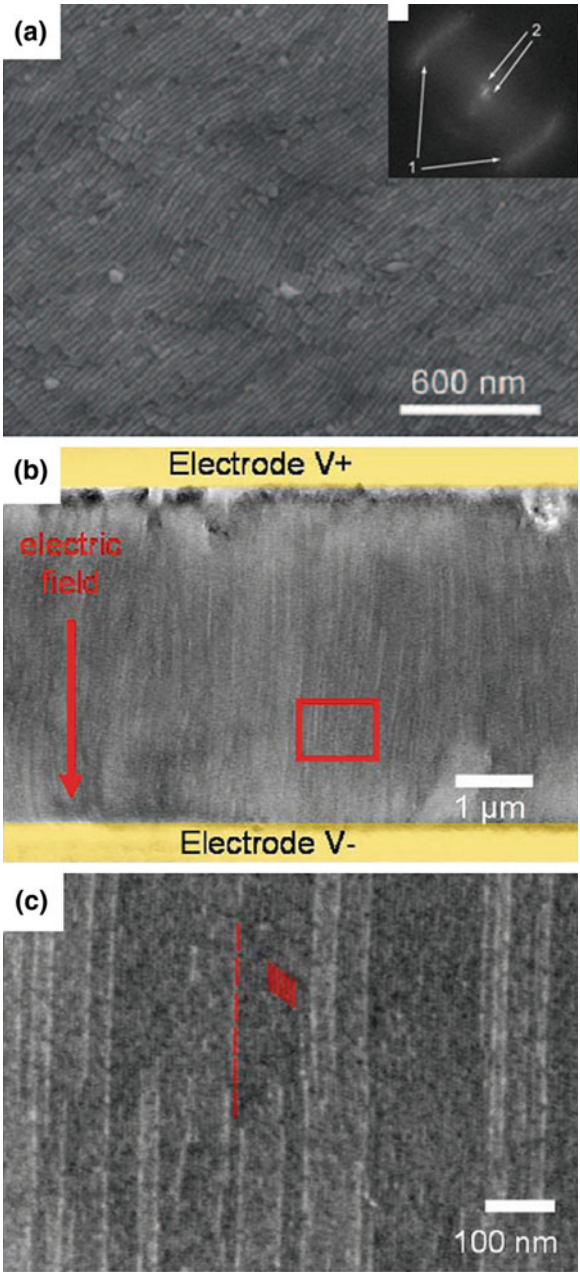

Fig. 2.12 **a** SEM image of Au nanorod multiplayers in nematic alignment. The corresponding FFT pattern in the *inset* shows single-direction diffuse streaks, suggesting only the orientational order but no translational order. Reproduced with permission from [94]. **b**, **c** SEM images of CdSe@CdS nanorod multiplayers in nematic alignment which are self-assembled in the electric field. The *red arrow* in **b** indicates the direction of the electric field, and the *red square* marks the region that is displayed in **c**. Some rods in **b** are highlighted in red as a guide to the eye. Reproduced with permission from [76]

colloidal solution, these polarized 1D nanocrystals tend to orient themselves along the direction of the field and form a nematic aligned structures. An example is illustrated by Manna and his colleagues, where asymmetric core-shell CdSe@CdS

nanorods were self-assembled in the electric field. The nanorods in between the electrodes were aligned uniformly over areas on the scale of tens of micrometers by following the field streamlines (Fig. 2.12b). The magnified view of a selected area (Fig. 2.12c) further indicated the nematic alignment [76]. It has shown that, even with a rather small dipole moment, the presence of sufficient anisotropy in the nanocrystal morphology can induce the ordering in orientation [104].

2.3.3.2 Smectic Alignment

"Smectic" is another term used frequently in liquid crystal field to describing a distinct ordered phase. Molecules in the smectic liquid crystals enjoy a general orientational order in the longitudinal direction like the nematic liquid crystals. In the transverse direction, they tend to organize into well-defined layers and exhibit a translational order. These layers can slide over one another as one entity. However, movement is restricted for molecules to cross the layers. Similar to the term "nematic", "smectic" has also been borrowed to describe some of close-packed multilayer structures from 1D building blocks. The 1D nanocrystals show remarkable similarity to the liquid modules and can be self-assembled into structures resembling smectic liquid crystals. A typical example of smectic aligned nanorods is presented in Fig. 2.13a. The longitudinal axes of Au nanorods are aligned roughly parallel to each other. In the transverse direction, the nanorods form separated layers that positioned to one direction. There is twofold of ordering for the smectic alignment as indicated by two-direction diffuse streaks in the FFT pattern (Fig. 2.13a inset). The parallel alignment of Au nanorods in the longitudinal direction is reflected by two diffuse streaks marked with arrow 3; while the layer-by-layer stacking in the transverse direction is reflected by an orthogonal set of streaks as marked with arrow 4 [94]. Talapin has further elucidated an antiparallel organization for the smectic multilayer structure that based on the attractive dipole interactions. For instance, the CdSe nanorods, which possessed large permanent dipole along the longitudinal axes, were able to be close-packed into smectic multilayers. The attractive dipole interactions were the driving forces and responsible for such alignment. The pairing of dipole moments required an antiparallel organization of neighboring nanorods within a layer and between adjacent layers (Fig. 2.13b) [74]. The Monte Carlo simulations for hard spherocylinders show the antiparallel organization is energetically favorable and can stabilize the smectic alignment. The smectic alignment can also be considered as 3D assembly of nanocrystals in two steps. The nanorods/nanowires are first assembled together in a side-by-side pattern to form layers. These layers are then stacked together, nearly parallel to each other, into a 3D structure.

The smectic alignment shares a lot of similarities with nematic alignment, and often case, both alignments can be achieved with same materials upon a slight change of experiment settings. According to the Onsager's hard-rod model [170, 171], 1D nanocrystals interacting with repulsive forces can display nematic

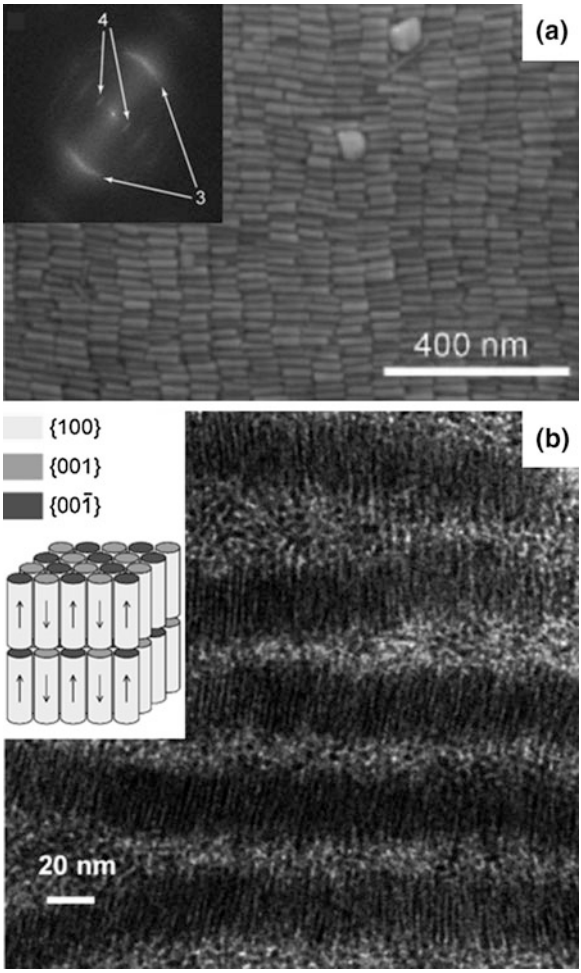

Fig. 2.13 **a** SEM image of Au nanorod multilayers in smectic alignment. The corresponding FFT pattern in the *inset* shows two-direction diffuse streaks, suggesting both orientational and translational order. Reproduced with permission from [94]. **b** TEM image of CdSe nanorod multilayers in smectic alignment. The antiparallel organization of nanorods in the *inset* shows a possible energetically favorable orientation to pair dipole moments both within and across layers. Reproduced with permission from [74]

alignment at low packing density. The anisotropic nanocrystals favor the parallel ordering as it increases the translational entropy by minimizing the excluded volume from the adjacent 1D nanocrystals. The sacrifice of orientational entropy can be compensated by the increase in the translational entropy. Frenkel's later computer simulation has demonstrated upon the increase of packing density, a thermodynamically stable smectic alignment is instead developed in the colloidal system with predominantly repulsive interactions. Apart from the packing density, the formation of nematic or smectic alignment is found experimentally aspect-ratio dependent as well. Long 1D nanocrystals (aspect ratio >7) tend to form nematic alignment while smectic alignment is favorable for short ones [78].

2.3.3.3 AB Stacking of Vertical Alignments

The AB stacking of vertical alignments is a 3D close-packed organization, which is composed of multiple vertically aligned layers that stacked in an end-to-end fashion. The alternating layers in the AB stacking structures have exactly the same organization within layers, however, with a rotational or lateral displacement across layers. The self-assembly of AB stacking structures is considered to start with the formation of individual vertically aligned monolayers. The vertically aligned monolayers are usually in the form of honeycomb structures (see vertical alignment for more details). When depositing such monolayers sequentially, a multilayer is expected which results from the layer-by-layer stacking. The stacking of vertical aligned monolayers maintains their original alignments, but creates diverse 3D arrangements. Typically, 3D stacking of nanorods is routinely observed when the concentration of 1D nanocrystals in solution is high [102]. A four-layer structure is shown in the SEM image in Fig. 2.14. Each layer by itself is an individual continuous 2D planar structure and the rods at the edges are perfectly orthogonal to the substrate, suggesting monolayers are preassembled before the multilayer structures [89]. This is further evidenced in experiments as both monolayers and multilayers are observed at the same time [172]. For AB stacking multilayers TEM images, a typical interference pattern can be observed due to the superimposition from two overlapping vertically aligned honeycomb structures. The AB stacking with a misorientation angle and/or lateral displacement from the two layers is the primary reason in causing such periodic effects when viewing two layers simultaneously in transmission mode. This further manifests a rotational and/or translational movement exist between the AB stacked layers [165].

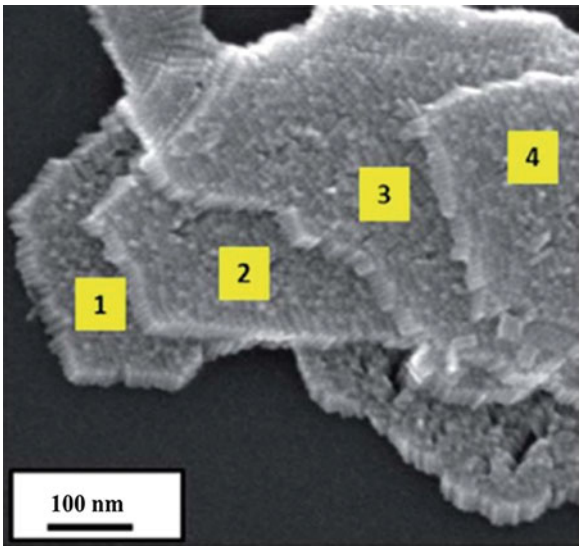

Fig. 2.14 SEM image of a four-layer CdS nanorod structure by AB stacking of vertical alignments. Reproduced with permission from [89]

Many self-assembled multilayer structures are based on a close-packing of building blocks, with the incoming building blocks filling the spaces between the previous assembled ones. For instance, the *fcc* and *hcp* patterns for the spherical nanocrystal self-assemblies are aligned upon one sheet of spheres arranged at the interstices of triangular bases from the underlying sheet. The vertically aligned monolayer, generally, is flat at the top and bottom surfaces and does not have obvious spacing. The 3D stacking pattern of monolayers from 1D nanocrystals therefore possesses more degrees of freedom than spherical building blocks. The incoming layer is less restricted and able to have both rotational and translation movements over the underlying base layer. The actual lateral displacement can be determined from TEM images while the misorientation angle can be obtained with the help from corresponding FFT or SAED patterns. There are generally two sets of spots in the electron diffraction patterns that arise from different orientated layers; and measuring the rotational deviation between them gives the misorientation angle. For honeycomb structures, the hexagonal symmetry in the monolayer means that every 30° rotation is a period. The exact structure of AB stacking of honeycomb structures has been studied comprehensively by Ryan and coworkers using STEM. When there was no offset in the overlapping layers, the TEM image (Fig. 2.15a) remained as a typical honeycomb packing pattern. However, the moiré fringe emerged when a misorientation angle existed between stacked layers (Fig. 2.15b–d). The interference appeared as a repeating hexagonal motif, with the size inversely proportional to the misorientation angle. As the angle offset increased to 29°, near to one period of 30°, a 12-fold ordering was seen (Fig. 2.15d), suggesting the rotational symmetry but no translational symmetry. A different interference pattern occured when a lateral displacement existed between the stacking layers (Fig. 2.15e, f). Only one hexagonal pattern was seen in the FFT pattern (Fig. 2.15e inset), suggesting the hexagonal symmetry of individual monolayer was kept intact, and further confirming the monolayer was preassembled before the stacking [173].

2.3.3.4 3D Assemblies

Other than nematic, smectic and AB stacking of vertical alignments, 1D nanocrystals can be self-assembled into other close-pack multilayer structures, which are termed as 3D assemblies here. 3D assemblies exist in many shapes, such as sphere, cylinder, and are difficult to realize compared with other packing alignments. The studies of complex 3D assemblies started from isotropic building blocks. Han's group has reported an oriented self-assembly of nanoparticles into uniform ellipsoidal structure [174], in which all the building blocks were aligned in the same facet orientation (identical crystallographic directions in all three dimensions). The resultant self-assembly appeared as monocrystalline structure in SEAD and HRTEM investigations. The facile desorption and exchange of capping ligands facilitated direct interactions between nanoparticles and led to orientated attachment of nanoparticle to form ellipsoidal structure.

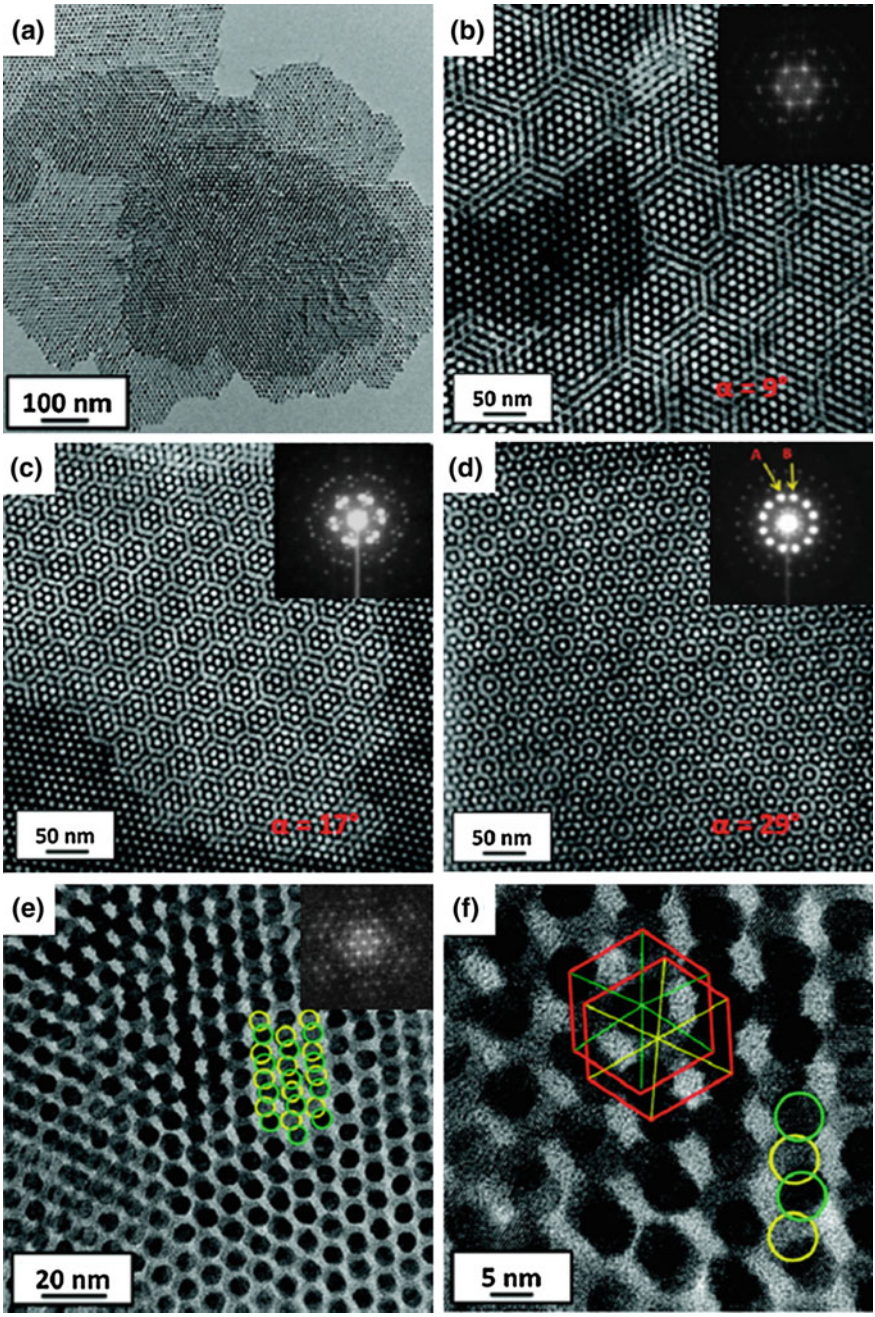
(a)
100 nm
(b)
50 nm
α = 9°
(c)
50 nm
α = 17°
(d)
A
B
50 nm
α = 29°
(e)
20 nm
(f)
5 nm

◀ **Fig. 2.15** TEM images, FFT and SAED patterns of CdS nanorod multiplayers by AB stacking of vertical alignments. **a** TEM images showing honeycomb packing when two layers are stacked perfectly. **b–d** DF-STEM images and corresponding FFT and SAED patterns (*insets*) showing Moiré fringes when two layers are stacked at a misorientation angle: **b** ~9°, **c** ~17°, **d** ~29°. **e**, **f** TEM and HRTEM images showing interference when two layers are stacked with lateral displacement. The FFT in **e** *inset* displays only one set of hexagonal diffraction spots. Reproduced with permission from [173]

Hollow spherical assemblies, such as micelle and vesicle, are one of the common 3D assemblies from 1D building blocks. Kumacheva and coworkers have reported a hollow spherical assembly by using Au nanorods. As shown in Fig. 2.16a, b, the walls of these spheres were composed of a single layer of Au nanorods, and the side-to-side spacing between the nanorods remained approximately at 5.3 nm. The cylindrical surfaces of the Au nanorods were exposed to the surroundings while the two ends were interconnected with neighboring nanorods. Similar to the isotropic building blocks, the surface chemistry played an important role in self-assembling such alignment. Showing in Fig. 2.16a, the cylindrical surfaces of Au nanorods were coated with a double layer of cetyl trimethylammonium bromide (CTAB), while the two ends of nanorods were anchored with thiol-terminated polystyrene molecules. This ligands coating essentially formed a hydrophilic gold nanorod tethered with a hydrophobic homopolymer at both ends. When adding water into the stock solution and incubating, these amphiphilic nanorods tended to interconnect at the ends to reduce the exposure of hydrophobic chain into water. By further assembling into sphere, they could minimize such exposures and interfacial energy, reaching a thermodynamically favored structure [138].

Recently, Cao's group has reported solid self-assembled structures with multiple well-defined supercrystalline domains, which open up new avenues for aligning 1D nanocrystals into more complex structures. These multiple domains structures were self-assembled in solution from highly fluorescent CdSe-CdS nanorods with their configurations and sizes dependent on the total number (N_t) of constituent nanorods

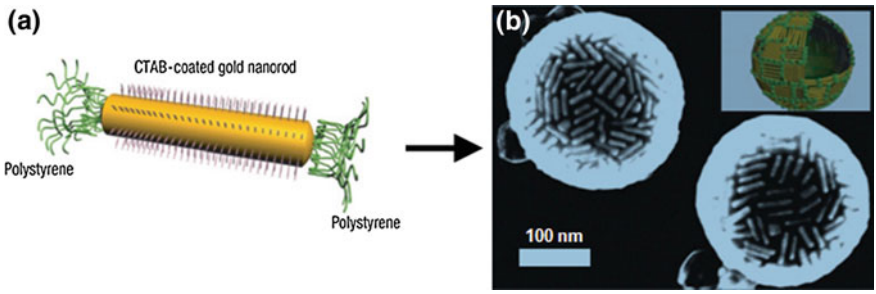

Fig. 2.16 **a** Schematic diagram of polymer-tethered gold nanorods. **b** SEM image of the hollow spherical self-assemblies obtained in the ternary dimethyl formamide/tetrahydrofuran/water mixture. The *inset* shows corresponding schematic diagram of the nanorod assemblies. Reproduced with permission from [138]

inside each self-assembly. For a regular double-domed cylinder structure, N_t needed to be less than ~80,000. Different from above-mentioned self-assembled structures, this double-domed cylinder itself consisted of seven distinct domains: the central cylinder, two domes at the top and bottom of cylinder, and four corners. The cylinder and two domes were comprised of multiple layers in AB stacking of vertical alignments, where the cylinder domain occupied a larger volume than that of corresponding domes. The four corners had their constituent nanorods aligned parallel to the electron beam and therefore these nanorods were seen as dots in the TEM images. In general, the longitudinal axes of nanorods within each domain were aligned parallel to each other, where the longitudinal axes of nanorods from two neighboring domains were aligned perpendicular to each other. The building blocks in this self-assembly possessed certain degrees of freedom (largely due to the rotational freedom around the longitudinal axes) as the corresponding SAED data showing ring or arc patterns. This internal organization of double-domed cylinders was further affirmed by the SAXS data. Two types of peaks were identified and corresponded to: (1) layer-to-layer periodicity from neighboring layers along rod longitudinal direction, (2) rod-to-rod periodicity within the same layer perpendicular to rod longitudinal direction. By varying incubating solvent, Cao's group has also demonstrated the formation of single-domain, needle-like self-assemblies [175, 176].

2.4 Summary and Outlook

In recent years, the self-assembly of 1D nanocrystals have become one of the most prominent fields for the nanoscience research and applications. The ability to organize and integrate small dimensional building blocks into large-area functional assemblies is an indispensible piece in incorporating nanotechnology into practical innovations. The self-assembled structures can possess unique properties that differ from the original building blocks. Different applications based on the optical, electronic, magnetic properties [82] of the self-assemblies are demonstrated. In particular, 1D nanocrystals, due to anisotropic structural properties, exhibit both challenges for self-assembling techniques as well as fascinating properties that appeal broad research interest. 1D nanocrystals, especially nanorods and nanowires, are shown here to be assembled via evaporation-mediated, electric-field-assisted and template-assisted assemblies on substrates. The evaporation-mediated self-assembly can strengthen the relatively weak attraction forces and help 1D nanocrystals aggregate together to minimize the free energy. The electric-field-assisted and template-assisted assembly is able to make use of external facilitations and induce building blocks orientated according to electric fields or template constrains. In the case of self-assembly at interfaces, the alignment of 1D nanocrystals leads to a reduction of total interfacial energy and drives them into ordered structures. The self-assembly in solutions is also demonstrated, which utilizes the chemical interactions in between 1D nanocrystals, capping ligands and solvents. Distinct from

isotropic building blocks, the self-assemblies of 1D nanocrystals display a number of different assembled structures. The 1D nanocrystals can form non-close-packed structures, such as stripes in both end-to-end and side-by-side alignments. The close-packed structures, in the other hand, exist in the form of monolayers or multilayers. A horizontal or vertical alignment is observed for the basic monolayer assemblies; while nematic, smectic, AB stacking of vertical alignments, and 3D assemblies are seen for the organization of 1D nanocrystals into multilayer structures. The self-assembly of 1D nanocrystals has gradually evolved into a versatile tool that could ultimately form tailored structures using specific approaches.

Looking ahead, the self-assembly of 1D nanocrystals will be the next step of nanofabrication for future technological innovations. It is a bottom up approach that is inexpensive and operates at smaller dimensions than current lithography based techniques. However, comparing to the patterned structures that built upon lithography, the self-assembled structures are prone to defects and the sizes of most assemblies are limited to micrometer range. The abilities to create centimeter-scale and defect-free nanocrystals assemblies are crucial for the development of reliable devices and shall be major focus in industrial applications. Meanwhile, the current self-assembly methods require the building blocks to be mono-dispersed. The restriction on the uniformity hinders the assembling of 1D nanocrystals with different sizes and shapes. The early attempts on binary 1D building blocks reported so far, usually find a phase separation of binary mixture instead of blended self-assembled patterns [94, 137, 177]. The fields that self-assemble two or more components with different chemical compositions still remain unexplored. A patterned structure with different chemical compositions now can only be obtained from physical methods, e.g, lithography, nanoimprinting. In addition, self-assembly of 1D nanocrystals utilizing magnetic field has seldom been reported. As a comparison, spherical nanoparticles are often demonstrated to be aligned in the external magnetic field. The 1D nanocrystals, due to the shape anisotropy, actually induce magnetic anisotropy that would open a new window to self-assemble 1D building blocks. In general, the self-assembly of 1D nanocrystals is still at its early stage of research and needs a better understanding towards the assembly mechanisms and structure-property relationships. Further comprehensive studies are required to find out simple and versatile methods that can create complicated, large-scale and defect-free self-assembled functional hierarchical architectures.

References

1. V.F. Puntes, K.M. Krishnan, A.P. Alivisatos, Colloidal nanocrystal shape and size control: the case of cobalt. Science **291**, 2115–2117 (2001)
2. J.J. Li, Y.A. Wang, W. Guo, J.C. Keay, T.D. Mishima, M.B. Johnson, X. Peng, Large-scale synthesis of nearly monodisperse CdSe/CdS core/shell nanocrystals using air-stable reagents via successive ion layer adsorption and reaction. J. Am. Chem. Soc. **125**, 12567–12575 (2003)

3. X. Wang, J. Zhuang, Q. Peng, Y. Li, A general strategy for nanocrystal synthesis. Nature **437**, 121–124 (2005)
4. Y. Yin, A.P. Alivisatos, Colloidal nanocrystal synthesis and the organic-inorganic interface. Nature **437**, 664–670 (2005)
5. Y. Xia, Y. Xiong, B. Lim, S.E. Skrabalak, Shape-controlled synthesis of metal nanocrystals: simple chemistry meets complex physics? Angew. Chem. Int. Ed. **48**, 60–103 (2009)
6. Z. Zhuang, Q. Peng, Y. Li, Controlled synthesis of semiconductor nanostructures in the liquid phase. Chem. Soc. Rev. **40**, 5492–5513 (2011)
7. K. Zhou, Y. Li, Catalysis based on nanocrystals with well-defined facets. Angew. Chem. Int. Ed. **51**, 602–613 (2012)
8. E. Ye, S.-Y. Zhang, S.H. Lim, M. Bosman, Z. Zhang, K.Y. Win, M.-Y. Han, Ternary Cobalt–iron phosphide nanocrystals with controlled compositions, properties, and morphologies from nanorods and nanorice to split nanostructures. Chem. Eur. J. **17**, 5982–5988 (2011)
9. S.-Y. Zhang, M.D. Regulacio, K.W. Shah, T. Sreethawong, Y. Zheng, M.-Y. Han, Colloidal preparation of monodisperse nanocrystals. J. Mol. Eng. Mater. **2**, 1430001 (2014)
10. P. Moriarty, Nanostructured materials. Rep. Prog. Phys. **64**, 297 (2001)
11. C.N.R. Rao, A.K. Cheetham, Science and technology of nanomaterials: current status and future prospects. J. Mater. Chem. **11**, 2887–2894 (2001)
12. M. Law, J. Goldberger, P. Yang, Semiconductor nanowires and nanotubes. Annu. Rev. Mater. Res. **34**, 83–122 (2004)
13. P.D. Cozzoli, T. Pellegrino, L. Manna, Synthesis, properties and perspectives of hybrid nanocrystal structures. Chem. Soc. Rev. **35**, 1195–1208 (2006)
14. Z.W. Seh, S. Liu, S.-Y. Zhang, M.S. Bharathi, H. Ramanarayan, M. Low, K.W. Shah, Y.-W. Zhang, M.-Y. Han, Anisotropic growth of titania onto various gold nanostructures: synthesis, theoretical understanding, and optimization for catalysis. Angew. Chem. Int. Ed. **50**, 10140–10143 (2011)
15. Z.W. Seh, S. Liu, S.-Y. Zhang, K.W. Shah, M.-Y. Han, Synthesis and multiple reuse of eccentric Au@TiO_2 nanostructures as catalysts. Chem. Commun. **47**, 6689–6691 (2011)
16. G. Wang, Q. Peng, Y. Li, Lanthanide-doped nanocrystals: synthesis, optical-magnetic properties, and applications. Acc. Chem. Res. **44**, 322–332 (2011)
17. G. Guan, S.-Y. Zhang, Y. Cai, S. Liu, M.S. Bharathi, M. Low, Y. Yu, J. Xie, Y. Zheng, Y.-W. Zhang, M.-Y. Han, Convenient purification of gold clusters by co-precipitation for improved sensing of hydrogen peroxide, mercury ions and pesticides. Chem. Commun. **50**, 5703–5705 (2014)
18. T. Sreethawong, K.W. Shah, S.-Y. Zhang, E. Ye, S.H. Lim, U. Maheswaran, W.Y. Mao, M.-Y. Han, Optimized production of copper nanostructures with high yields for efficient use as thermal conductivity-enhancing PCM dopant. J. Mater. Chem. A **2**, 3417–3423 (2014)
19. C.L. Choi, A.P. Alivisatos, From artificial atoms to nanocrystal molecules: preparation and properties of more complex nanostructures. Annu. Rev. Phys. Chem. **61**, 369–389 (2010)
20. M. Grzelczak, J. Vermant, E.M. Furst, L.M. Liz-Marzán, Directed self-assembly of nanoparticles. ACS Nano **4**, 3591–3605 (2010)
21. M.P. Pileni, Inorganic nanocrystals self ordered in 2D superlattices: how versatile are the physical and chemical properties? Phys. Chem. Chem. Phys. **12**, 11821–11835 (2010)
22. Z. Quan, J. Fang, Superlattices with non-spherical building blocks. Nano Today **5**, 390–411 (2010)
23. M.R. Jones, K.D. Osberg, R.J. Macfarlane, M.R. Langille, C.A. Mirkin, Templated techniques for the synthesis and assembly of plasmonic nanostructures. Chem. Rev. **111**, 3736–3827 (2011)
24. T. Wang, D. LaMontagne, J. Lynch, J. Zhuang, Y.C. Cao, Colloidal superparticles from nanoparticle assembly. Chem. Soc. Rev. **42**, 2804–2823 (2013)
25. S.-Y. Zhang, M.D. Regulacio, M.-Y. Han, Self-assembly of colloidal one-dimensional nanocrystals. Chem. Soc. Rev. **43**, 2301–2323 (2014)

26. P. Bartlett, R.H. Ottewill, P.N. Pusey, Superlattice formation in binary mixtures of hard-sphere colloids. Phys. Rev. Lett. **68**, 3801–3804 (1992)
27. C.P. Collier, T. Vossmeyer, J.R. Heath, Nanocrystal superlattices. Annu. Rev. Phys. Chem. **49**, 371–404 (1998)
28. C.B. Murray, C.R. Kagan, M.G. Bawendi, Snthesis and characterization of monodisperse nanocrystals and close-packed nanocrystal assemblies. Annu. Rev. Mater. Sci. **30**, 545–610 (2000)
29. T.K. Sau, C.J. Murphy, Self-assembly patterns formed upon solvent evaporation of aqueous cetyltrimethylammonium bromide-coated gold nanoparticles of various shapes. Langmuir **21**, 2923–2929 (2005)
30. K.C. Ng, I.B. Udagedara, I.D. Rukhlenko, Y. Chen, Y. Tang, M. Premaratne, W. Cheng, Free-standing plasmonic-nanorod superlattice sheets. ACS Nano **6**, 925–934 (2012)
31. T.S. Ahmadi, Z.L. Wang, T.C. Green, A. Henglein, M.A. El-Sayed, Shape-controlled synthesis of colloidal platinum nanoparticles. Science **272**, 1924–1925 (1996)
32. M. Brust, M. Walker, D. Bethell, D.J. Schiffrin, R. Whyman, Synthesis of thiol-derivatised gold nanoparticles in a two-phase Liquid-Liquid system. J. Chem. Soc. Chem. Commun. **1994**, 801–802 (1994)
33. M.-C. Daniel, D. Astruc, Gold nanoparticles: Assembly, supramolecular chemistry, quantum-size-related properties, and applications toward biology, catalysis, and nanotechnology. Chem. Rev. **104**, 293–346 (2004)
34. S. Sun, C.B. Murray, D. Weller, L. Folks, A. Moser, Monodisperse FePt nanoparticles and ferromagnetic FePt nanocrystal superlattices. Science **287**, 1989–1992 (2000)
35. Y. Sun, Y. Xia, Shape-controlled synthesis of gold and silver nanoparticles. Science **298**, 2176–2179 (2002)
36. S.-H. Liu, H. Gao, E. Ye, M. Low, S.H. Lim, S.-Y. Zhang, X. Lieu, S. Tripathy, W. Tremel, M.-Y. Han, Graphitically encapsulated cobalt nanocrystal assemblies. Chem. Commun. **46**, 4749–4751 (2010)
37. E. Ye, S.-Y. Zhang, S. Liu, M.-Y. Han, Disproportionation for growing copper nanowires and their controlled self-assembly facilitated by ligand exchange. Chem. Eur. J. **17**, 3074–3077 (2011)
38. M. Bruchez, M. Moronne, P. Gin, S. Weiss, A.P. Alivisatos, Semiconductor nanocrystals as fluorescent biological labels. Science **281**, 2013–2016 (1998)
39. T. Trindade, P. O'Brien, N.L. Pickett, Nanocrystalline semiconductors: synthesis, properties, and perspectives. Chem. Mater. **13**, 3843–3858 (2001)
40. E.A. Meulenkamp, Synthesis and growth of ZnO nanoparticles. J. Phys. Chem. B **102**, 5566–5572 (1998)
41. S. Sun, H. Zeng, Size-controlled synthesis of magnetite nanoparticles. J. Am. Chem. Soc. **124**, 8204–8205 (2002)
42. E. Ye, S.-Y. Zhang, S.H. Lim, S. Liu, M.-Y. Han, Morphological tuning, self-assembly and optical properties of indium oxide nanocrystals. Phys. Chem. Chem. Phys. **12**, 11923–11929 (2010)
43. S. Vaucher, M. Li, S. Mann, Synthesis of prussian blue nanoparticles and nanocrystal superlattices in reverse microemulsions. Angew. Chem. Int. Ed. **39**, 1793–1796 (2000)
44. C.R. Martin, Nanomaterials: a membrane-based synthetic approach. Science **266**, 1961–1966 (1994)
45. A. Stein, R.C. Schroden, Colloidal crystal templating of three-dimensionally ordered macroporous solids: materials for photonics and beyond. Curr. Opin. Solid State Mater. Sci. **5**, 553–564 (2001)
46. B. Amir Parviz, D. Ryan, and G.M. Whitesides, Using self-assembly for the fabrication of nano-scale electronic and photonic devices. IEEE Trans. Adv. Pack. **26**, 233–241 (2003)
47. C.J. Murphy, T.K. Sau, A.M. Gole, C.J. Orendorff, J. Gao, L. Gou, S.E. Hunyadi, T. Li, Anisotropic metal nanoparticles: synthesis, assembly, and optical applications. J. Phys. Chem. B **109**, 13857–13870 (2005)

48. C. Nobile, V.A. Fonoberov, S. Kudera, A. Della Torre, A. Ruffino, G. Chilla, T. Kipp, D. Heitmann, L. Manna, R. Cingolani, A.A. Balandin, R. Krahne, Confined optical phonon modes in aligned nanorod arrays detected by resonant inelastic light scattering. Nano Lett. **7**, 476–479 (2007)
49. A. Rizzo, C. Nobile, M. Mazzeo, M.D. Giorgi, A. Fiore, L. Carbone, R. Cingolani, L. Manna, G. Gigli, Polarized light emitting diode by long-range nanorod self-assembling on a water surface. ACS Nano **3**, 1506–1512 (2009)
50. D. Vennerberg, Z. Lin, Upconversion nanocrystals: synthesis, properties, assembly and applications. Sci. Adv. Mater. **3**, 26–40 (2011)
51. S.A. Maier, M.L. Brongersma, P.G. Kik, S. Meltzer, A.A. G. Requicha, B.E. Koel, H.A. Atwater, Plasmonics—a route to nanoscale optical devices (Adv. Mater. **13**, 1501 (2001)), Adv. Mater. (Weinheim, Ger.) **15**, 562–562 (2003)
52. S.A. Maier, P.G. Kik, H.A. Atwater, S. Meltzer, E. Harel, B.E. Koel, A.A.G. Requicha, Local detection of electromagnetic energy transport below the diffraction limit in metal nanoparticle plasmon waveguides. Nat. Mater. **2**, 229–232 (2003)
53. M. Rycenga, C.M. Cobley, J. Zeng, W. Li, C.H. Moran, Q. Zhang, D. Qin, Y. Xia, Controlling the synthesis and assembly of silver nanostructures for plasmonic applications. Chem. Rev. **111**, 3669–3712 (2011)
54. A. Tao, F. Kim, C. Hess, J. Goldberger, R. He, Y. Sun, Y. Xia, P. Yang, Langmuir–Blodgett silver nanowire monolayers for molecular sensing using surface-enhanced Raman spectroscopy. Nano Lett. **3**, 1229–1233 (2003)
55. J. Fang, S. Du, S. Lebedkin, Z. Li, R. Kruk, M. Kappes, H. Hahn, Gold mesostructures with tailored surface topography and their self-assembly arrays for surface-enhanced Raman spectroscopy. Nano Lett. **10**, 5006–5013 (2010)
56. A. Chen, A.E. DePrince, A. Demortière, A. Joshi-Imre, E.V. Shevchenko, S.K. Gray, U. Welp, V.K. Vlasko-Vlasov, Self-assembled large Au nanoparticle arrays with regular hot spots for SERS. Small **7**, 2365–2371 (2011)
57. X.-Z. Shi, C.-M. Shen, D.-K. Wang, C. Li, Y. Tian, Z.-C. Xu, C.-M. Wang, H.-J. Gao, Surface-enhanced Raman scattering properties of highly ordered self-assemblies of gold nanorods with different aspect ratios. Chin. Phys. B **20**, 076103 (2011)
58. T.S. Sreeprasad, T. Pradeep, Reversible assembly and disassembly of gold nanorods induced by EDTA and its application in SERS tuning. Langmuir **27**, 3381–3390 (2011)
59. Z. Zhu, H. Meng, W. Liu, X. Liu, J. Gong, X. Qiu, L. Jiang, D. Wang, Z. Tang, Superstructures and SERS properties of gold nanocrystals with different shapes. Angew. Chem. Int. Ed. **50**, 1593–1596 (2011)
60. S. Sun, C.B. Murray, Synthesis of monodisperse cobalt nanocrystals and their assembly into magnetic superlattices. J. Appl. Phys. **85**, 4325–4330 (1999)
61. S. Behrens, Preparation of functional magnetic nanocomposites and hybrid materials: recent progress and future directions. Nanoscale **3**, 877–892 (2011)
62. D. Whang, S. Jin, Y. Wu, C.M. Lieber, Large-scale hierarchical organization of nanowire arrays for integrated nanosystems. Nano Lett. **3**, 1255–1259 (2003)
63. D.V. Talapin, J.-S. Lee, M.V. Kovalenko, E.V. Shevchenko, Prospects of colloidal nanocrystals for electronic and optoelectronic applications. Chem. Rev. **110**, 389–458 (2010)
64. I.J. Kramer, E.H. Sargent, Colloidal quantum dot photovoltaics: a path forward. ACS Nano **5**, 8506–8514 (2011)
65. Z.-Y. Zhou, N. Tian, J.-T. Li, I. Broadwell, S.-G. Sun, Nanomaterials of high surface energy with exceptional properties in catalysis and energy storage. Chem. Soc. Rev. **40**, 4167–4185 (2011)
66. W. Lu, J. Fang, K.L. Stokes, J. Lin, Shape evolution and self assembly of monodisperse PbTe nanocrystals. J. Am. Chem. Soc. **126**, 11798–11799 (2004)
67. J. Zhang, A. Kumbhar, J. He, N.C. Das, K. Yang, J.-Q. Wang, H. Wang, K.L. Stokes, J. Fang, Simple cubic super crystals containing PbTe nanocubes and their core–shell building blocks. J. Am. Chem. Soc. **130**, 15203–15209 (2008)

68. L. Motte, F. Billoudet, E. Lacaze, M.-P. Pileni, Self-organization of size-selected, nanoparticles into three-dimensional superlattices. Adv. Mater. **8**, 1018–1020 (1996)
69. T. Mokari, M. Zhang, P. Yang, Shape, size, and assembly control of PbTe nanocrystals. J. Am. Chem. Soc. **129**, 9864–9865 (2007)
70. J. Zhuang, H. Wu, Y. Yang, Y.C. Cao, Supercrystalline colloidal particles from artificial atoms. J. Am. Chem. Soc. **129**, 14166–14167 (2007)
71. A. Demortière, P. Launois, N. Goubet, P.A. Albouy, C. Petit, Shape-controlled platinum nanocubes and their assembly into two-dimensional and three-dimensional superlattices. J. Phys. Chem. B **112**, 14583–14592 (2008)
72. M. Pang, H.C. Zeng, Highly ordered self-assemblies of submicrometer Cu_2O spheres and their hollow chalcogenide derivatives. Langmuir **26**, 5963–5970 (2010)
73. K.X. Yao, X.M. Yin, T.H. Wang, H.C. Zeng, Synthesis, self-assembly, disassembly, and reassembly of two types of Cu_2O nanocrystals unifaceted with 001 or 110 planes. J. Am. Chem. Soc. **132**, 6131–6144 (2010)
74. D.V. Talapin, E.V. Shevchenko, C.B. Murray, A. Kornowski, S. Förster, H. Weller, CdSe and CdSe/CdS nanorod solids. J. Am. Chem. Soc. **126**, 12984–12988 (2004)
75. S. Ahmed, K.M. Ryan, Self-assembly of vertically aligned nanorod supercrystals using highly oriented pyrolytic graphite. Nano Lett. **7**, 2480–2485 (2007)
76. L. Carbone, C. Nobile, M. De Giorgi, F.D. Sala, G. Morello, P. Pompa, M. Hytch, E. Snoeck, A. Fiore, I.R. Franchini, M. Nadasan, A.F. Silvestre, L. Chiodo, S. Kudera, R. Cingolani, R. Krahne, L. Manna, Synthesis and micrometer-scale assembly of colloidal CdSe/CdS nanorods prepared by a seeded growth approach. Nano Lett. **7**, 2942–2950 (2007)
77. W. Lu, Q. Liu, Z. Sun, J. He, C. Ezeolu, J. Fang, Super crystal structures of octahedral c-In_2O_3 nanocrystals. J. Am. Chem. Soc. **130**, 6983–6991 (2008)
78. N.R. Jana, Shape effect in nanoparticle self-assembly. Angew. Chem. Int. Ed. **43**, 1536–1540 (2004)
79. C.B. Murray, S. Sun, W. Gaschler, H. Doyle, T.A. Betley, C.R. Kagan, Colloidal synthesis of nanocrystals and nanocrystal superlattices. IBM J. Res. Dev. **45**, 47–56 (2001)
80. M.P. Pileni, Nanocrystal self-assemblies: fabrication and collective properties. J. Phys. Chem. B **105**, 3358–3371 (2001)
81. A.L. Rogach, D.V. Talapin, E.V. Shevchenko, A. Kornowski, M. Haase, H. Weller, Organization of matter on different size scales: monodisperse nanocrystals and their superstructures. Adv. Funct. Mater. **12**, 653–664 (2002)
82. S. Kinge, M. Crego-Calama, D.N. Reinhoudt, Self-assembling nanoparticles at surfaces and interfaces. ChemPhysChem **9**, 20–42 (2008)
83. Y. Min, M. Akbulut, K. Kristiansen, Y. Golan, J. Israelachvili, The role of interparticle and external forces in nanoparticle assembly. Nat. Mater. **7**, 527–538 (2008)
84. Y. Ofir, B. Samanta, V.M. Rotello, Polymer and biopolymer mediated self-assembly of gold nanoparticles. Chem. Soc. Rev. **37**, 1814–1825 (2008)
85. K.J.M. Bishop, C.E. Wilmer, S. Soh, B.A. Grzybowski, Nanoscale forces and their uses in self-assembly. Small **5**, 1600–1630 (2009)
86. Y. Nagaoka, O. Chen, Z. Wang, Y.C. Cao, Structural control of nanocrystal superlattices using organic guest molecules. J. Am. Chem. Soc. **134**, 2868–2871 (2012)
87. T. Wang, X. Wang, D. LaMontagne, Z. Wang, Z. Wang, Y.C. Cao, Shape-controlled synthesis of colloidal superparticles from nanocubes. J. Am. Chem. Soc. **134**, 18225–18228 (2012)
88. M.D. Bentzon, J. van Wonterghem, S. Mørup, A. Thölén, C.J.W. Koch, Ordered aggregates of ultrafine iron oxide particles: 'super crystals'. Philos. Mag. B **60**, 169–178 (1989)
89. A. Singh, R.D. Gunning, S. Ahmed, C.A. Barrett, N.J. English, J.-A. Garate, K.M. Ryan, Controlled semiconductor nanorod assembly from solution: influence of concentration, charge and solvent nature. J. Mater. Chem. **22**, 1562–1569 (2012)
90. W.M. Gelbart, R.P. Sear, J.R. Heath, S. Chaney, Array formation in nano-colloids: theory and experiment in 2D. Faraday Discuss. **112**, 299–307 (1999)

91. E. Rabani, D.R. Reichman, P.L. Geissler, L.E. Brus, Drying-mediated self-assembly of nanoparticles. Nature **426**, 271–274 (2003)
92. G. Yosef, E. Rabani, Self-assembly of nanoparticles into rings: a lattice-gas model. J. Phys. Chem. B **110**, 20965–20972 (2006)
93. J.L. Baker, A. Widmer-Cooper, M.F. Toney, P.L. Geissler, A.P. Alivisatos, Device-scale perpendicular alignment of colloidal nanorods. Nano Lett. **10**, 195–201 (2010)
94. T. Ming, X. Kou, H. Chen, T. Wang, H.-L. Tam, K.-W. Cheah, J.-Y. Chen, J. Wang, Ordered gold nanostructure assemblies formed by droplet evaporation. Angew. Chem. Int. Ed. **47**, 9685–9690 (2008)
95. D. Bargeman, F. van Voorst Vader, Van der waals forces between immersed particles, J. Electr. Chem. Interf. Electrochem. **37**, 45–52 (1972)
96. B. Nikoobakht, Z.L. Wang, M.A. El-Sayed, Self-assembly of gold nanorods. J. Phys. Chem. B **104**, 8635–8640 (2000)
97. J. Kleinert, S. Kim, O.D. Velev, Electric-field-assisted convective assembly of colloidal crystal coatings. Langmuir **26**, 10380–10385 (2010)
98. P.A. Smith, C.D. Nordquist, T.N. Jackson, T.S. Mayer, B.R. Martin, J. Mbindyo, T.E. Mallouk, Electric-field assisted assembly and alignment of metallic nanowires. Appl. Phys. Lett. **77**, 1399–1401 (2000)
99. O. Harnack, C. Pacholski, H. Weller, A. Yasuda, J.M. Wessels, Rectifying behavior of electrically aligned ZnO nanorods. Nano Lett. **3**, 1097–1101 (2003)
100. S. Gupta, Q. Zhang, T. Emrick, T.P. Russell, "Self-corralling" nanorods under an applied electric field. Nano Lett. **6**, 2066–2069 (2006)
101. Z. Hu, M.D. Fischbein, C. Querner, M. Drndić, Electric-field-driven accumulation and alignment of CdSe and CdTe nanorods in nanoscale devices. Nano Lett. **6**, 2585–2591 (2006)
102. K.M. Ryan, A. Mastroianni, K.A. Stancil, H. Liu, A.P. Alivisatos, Electric-field-assisted assembly of perpendicularly oriented nanorod superlattices. Nano Lett. **6**, 1479–1482 (2006)
103. M. Mittal, E.M. Furst, Electric field-directed convective assembly of ellipsoidal colloidal particles to create optically and mechanically anisotropic thin films. Adv. Funct. Mater. **19**, 3271–3278 (2009)
104. M. Zorn, M.N. Tahir, B. Bergmann, W. Tremel, C. Grigoriadis, G. Floudas, R. Zentel, Orientation and dynamics of ZnO nanorod liquid crystals in electric fields. Macromol. Rapid Commun. **31**, 1101–1107 (2010)
105. G. Michael, H. Michael, The preparation of ordered colloidal magnetic particles by magnetophoretic deposition. J. Phys. D Appl. Phys. **32**, L111 (1999)
106. J.O.M. Bockris, A.K.N. Reddy, M. Gamboa-Aldeco, M.E. Gamboa-Aldeco, *Modern Electrochemistry.* Springer, 2000
107. T. Vossmeyer, E. DeIonno, J.R. Heath, Light-directed assembly of nanoparticles. Angew. Chem. Int. Ed. Engl. **36**, 1080–1083 (1997)
108. T. Vossmeyer, S. Jia, E. DeIonno, M.R. Diehl, S.-H. Kim, X. Peng, A.P. Alivisatos, J.R. Heath, Combinatorial approaches toward patterning nanocrystals. J. Appl. Phys. **84**, 3664–3670 (1998)
109. H.X. He, H. Zhang, Q.G. Li, T. Zhu, S.F.Y. Li, Z.F. Liu, Fabrication of designed architectures of Au nanoparticles on solid substrate with printed self-assembled monolayers as templates. Langmuir **16**, 3846–3851 (2000)
110. F. Fan, K.J. Stebe, Size-selective deposition and sorting of lyophilic colloidal particles on surfaces of patterned wettability. Langmuir **21**, 1149–1152 (2005)
111. A. Akey, C. Lu, L. Yang, I.P. Herman, Formation of thick, large-area nanoparticle superlattices in lithographically defined geometries. Nano Lett. **10**, 1517–1521 (2010)
112. M. Artemyev, B. Möller, U. Woggon, Unidirectional alignment of CdSe nanorods. Nano Lett. **3**, 509–512 (2003)
113. S. Liu, J.B.H. Tok, J. Locklin, Z. Bao, Assembly and alignment of metallic nanorods on surfaces with patterned wettability. Small **2**, 1448–1453 (2006)

114. Q. Zhang, S. Gupta, T. Emrick, T.P. Russell, Surface-functionalized CdSe nanorods for assembly in diblock copolymer templates. J. Am. Chem. Soc. **128**, 3898–3899 (2006)
115. C. Hamon, M. Postic, E. Mazari, T. Bizien, C. Dupuis, P. Even-Hernandez, A. Jimenez, L. Courbin, C. Gosse, F. Artzner, V. Marchi-Artzner, Three-dimensional self-assembling of gold nanorods with controlled macroscopic shape and local smectic B order. ACS Nano **6**, 4137–4146 (2012)
116. C. Kuemin, L. Nowack, L. Bozano, N.D. Spencer, H. Wolf, Oriented assembly of gold nanorods on the single-particle level. Adv. Funct. Mater. **22**, 702–708 (2012)
117. A.P. Alivisatos, K.P. Johnsson, X. Peng, T.E. Wilson, C.J. Loweth, M.P. Bruchez, P.G. Schultz, Organization of 'nanocrystal molecules' using DNA. Nature **382**, 609–611 (1996)
118. E. Dujardin, L.-B. Hsin, C.R.C. Wang, S. Mann, DNA-driven self-assembly of gold nanorods. Chem. Commun. **2001**, 1264–1265 (2001)
119. B. Pan, L. Ao, F. Gao, H. Tian, R. He, D. Cui, End-to-end self-assembly and colorimetric characterization of gold nanorods and nanospheres via oligonucleotide hybridization. Nanotechnology **16**, 1776 (2005)
120. B. Pan, D. Cui, C. Ozkan, P. Xu, T. Huang, Q. Li, H. Chen, F. Liu, F. Gao, R. He, DNA-templated ordered array of gold nanorods in one and two dimensions. J. Phys. Chem. C **111**, 12572–12576 (2007)
121. H.-C. Huang, P. Koria, S.M. Parker, L. Selby, Z. Megeed, K. Rege, Optically responsive gold nanorod–polypeptide assemblies. Langmuir **24**, 14139–14144 (2008)
122. W. Cheng, M.J. Campolongo, J.J. Cha, S.J. Tan, C.C. Umbach, D.A. Muller, D. Luo, Free-standing nanoparticle superlattice sheets controlled by DNA. Nat. Mater. **8**, 519–525 (2009)
123. R. Iwaura, T. Iizawa, H. Minamikawa, M. Ohnishi-Kameyama, T. Shimizu, Diverse morphologies of self-assemblies from homoditopic 1,18-nucleotide-appended bolaamphiphiles: effects of nucleobases and complementary oligonucleotides. Small **6**, 1131–1139 (2010)
124. M.A. Correa-Duarte, J. Pérez-Juste, A. Sánchez-Iglesias, M. Giersig, L.M. Liz-Marzán, Aligning Au nanorods by using carbon nanotubes as templates. Angew. Chem. Int. Ed. **44**, 4375–4378 (2005)
125. E. Ploshnik, A. Salant, U. Banin, R. Shenhar, Hierarchical surface patterns of nanorods obtained by co-assembly with block copolymers in ultrathin films. Adv. Mater. **22**, 2774–2779 (2010)
126. E. Ploshnik, A. Salant, U. Banin, R. Shenhar, Co-assembly of block copolymers and nanorods in ultrathin films: effects of copolymer size and nanorod filling fraction. Phys. Chem. Chem. Phys. **12**, 11885–11893 (2010)
127. M.A. Modestino, E.R. Chan, A. Hexemer, J.J. Urban, R.A. Segalman, Controlling nanorod self-assembly in polymer thin films. Macromolecules **44**, 7364–7371 (2011)
128. K. Thorkelsson, A.J. Mastroianni, P. Ercius, T. Xu, Direct nanorod assembly using block copolymer-based supramolecules. Nano Lett. **12**, 498–504 (2011)
129. S.U. Pickering, CXCVI.-Emulsions. J. Chem. Soc. Trans. **91**, 2001–2021 (1907)
130. W. Ramsden, Separation of solids in the surface-layers of solutions and 'suspensions' (observations on surface-membranes, bubbles, emulsions, and mechanical coagulation).—preliminary account. Proc. R. Soc. Lond. **72**, 156–164 (1903)
131. P. Pieranski, Two-dimensional interfacial colloidal crystals. Phys. Rev. Lett. **45**, 569–572 (1980)
132. A. Boker, J. He, T. Emrick, T.P. Russell, Self-assembly of nanoparticles at interfaces. Soft Matter **3**, 1231–1248 (2007)
133. J. He, Q. Zhang, S. Gupta, T. Emrick, T.P. Russell, P. Thiyagarajan, Drying droplets: a window into the behavior of nanorods at interfaces. Small **3**, 1214–1217 (2007)
134. E.M. Furst, Directing colloidal assembly at fluid interfaces. Proc. Natl. Acad. Sci. U.S.A. **108**, 20853–20854 (2011)
135. F. Kim, S. Kwan, J. Akana, P. Yang, Langmuir–Blodgett nanorod assembly. J. Am. Chem. Soc. **123**, 4360–4361 (2001)

136. P. Yang, F. Kim, Langmuir-Blodgett assembly of one-dimensional nanostructures. ChemPhysChem **3**, 503–506 (2002)
137. N. Pradhan, S. Efrima, Supercrystals of uniform nanorods and nanowires, and the nanorod-to-nanowire oriented transition. J. Phys. Chem. B **108**, 11964–11970 (2004)
138. Z. Nie, D. Fava, E. Kumacheva, S. Zou, G.C. Walker, M. Rubinstein, Self-assembly of metal-polymer analogues of amphiphilic triblock copolymers. Nat. Mater. **6**, 609–614 (2007)
139. L.S. Li, A.P. Alivisatos, Semiconductor nanorod liquid crystals and their assembly on a substrate. Adv. Mater. **15**, 408–411 (2003)
140. K. Soulantica, A. Maisonnat, M.-C. Fromen, M.-J. Casanove, B. Chaudret, Spontaneous formation of ordered 3D superlattices of nanocrystals from polydisperse colloidal solutions. Angew. Chem. Int. Ed. **42**, 1945–1949 (2003)
141. H.-S. Park, A. Agarwal, N.A. Kotov, O.D. Lavrentovich, Controllable side-by-side and end-to-end assembly of Au nanorods by lyotropic chromonic materials. Langmuir **24**, 13833–13837 (2008)
142. T.S. Sreeprasad, A.K. Samal, T. Pradeep, One-, two-, and three-dimensional superstructures of gold nanorods induced by dimercaptosuccinic acid. Langmuir **24**, 4589–4599 (2008)
143. Z. Huo, C.-K. Tsung, W. Huang, M. Fardy, R. Yan, X. Zhang, Y. Li, P. Yang, Self-organized ultrathin oxide nanocrystals. Nano Lett. **9**, 1260–1264 (2009)
144. K.K. Caswell, J.N. Wilson, U.H.F. Bunz, C.J. Murphy, Preferential end-to-end assembly of gold nanorods by Biotin–Streptavidin connectors. J. Am. Chem. Soc. **125**, 13914–13915 (2003)
145. K.G. Thomas, S. Barazzouk, B.I. Ipe, S.T.S. Joseph, P.V. Kamat, Uniaxial plasmon coupling through longitudinal self-assembly of gold nanorods. J. Phys. Chem. B **108**, 13066–13068 (2004)
146. J.-Y. Chang, H. Wu, H. Chen, Y.-C. Ling, W. Tan, Oriented assembly of Au nanorods using biorecognition system. Chem. Commun. **2005**, 1092–1094 (2005)
147. X. Hu, W. Cheng, T. Wang, E. Wang, S. Dong, Well-ordered end-to-end linkage of gold nanorods. Nanotechnology **16**, 2164 (2005)
148. S.T. Shibu Joseph, B.I. Ipe, P. Pramod, K.G. Thomas, Gold nanorods to nanochains: mechanistic investigations on their longitudinal assembly using α,ω-alkanedithiols and interplasmon coupling. J. Phys. Chem. B **110**, 150–157 (2006)
149. P.K. Sudeep, S.T.S. Joseph, K.G. Thomas, Selective detection of cysteine and glutathione using gold nanorods. J. Am. Chem. Soc. **127**, 6516–6517 (2005)
150. M.H. Zareie, X. Xu, M.B. Cortie, In situ organization of gold nanorods on mixed self-assembled-monolayer substrates. Small **3**, 139–145 (2007)
151. S. Zhang, X. Kou, Z. Yang, Q. Shi, G.D. Stucky, L. Sun, J. Wang, C. Yan, Nanonecklaces assembled from gold rods, spheres, and bipyramids. Chem. Commun. **2007**, 1816–1818 (2007)
152. N.D. Denkov, O.D. Velev, P.A. Kralchevsky, I.B. Ivanov, H. Yoshimura, K. Nagayama, Two-dimensional crystallization. Nature **361**, 26–26 (1993)
153. F. Dumestre, B. Chaudret, C. Amiens, M. Respaud, P. Fejes, P. Renaud, P. Zurcher, Unprecedented crystalline super-lattices of monodisperse cobalt nanorods. Angew. Chem. Int. Ed. **42**, 5213–5216 (2003)
154. C.-C. Kang, C.-W. Lai, H.-C. Peng, J.-J. Shyue, P.-T. Chou, 2D self-bundled CdS nanorods with micrometer dimension in the absence of an external directing process. ACS Nano **2**, 750–756 (2008)
155. A.M. Hung, N.A. Konopliv, J.N. Cha, Solvent-based assembly of CdSe nanorods in solution. Langmuir **27**, 12322–12328 (2011)
156. W. Ni, R.A. Mosquera, J. Pérez-Juste, L.M. Liz-Marzán, Evidence for hydrogen-bonding-directed assembly of gold nanorods in aqueous solution. J. Phys. Chem. Lett. **1**, 1181–1185 (2010)
157. N. Zhao, K. Liu, J. Greener, Z. Nie, E. Kumacheva, Close-packed superlattices of side-by-side assembled Au-CdSe nanorods. Nano Lett. **9**, 3077–3081 (2009)

158. Z. Sun, W. Ni, Z. Yang, X. Kou, L. Li, J. Wang, pH-Controlled reversible assembly and disassembly of gold nanorods. Small **4**, 1287–1292 (2008)
159. S.-Y. Zhang, E. Ye, S. Liu, S.H. Lim, S.Y. Tee, Z. Dong, M.-Y. Han, Temperature and chemical bonding-directed self-assembly of cobalt phosphide nanowires in reaction solutions into vertical and horizontal alignments. Adv. Mater. **24**, 4369–4375 (2012)
160. C.J. Orendorff, P.L. Hankins, C.J. Murphy, pH-Triggered assembly of gold nanorods. Langmuir **21**, 2022–2026 (2005)
161. D. Baranov, A. Fiore, M. van Huis, C. Giannini, A. Falqui, U. Lafont, H. Zandbergen, M. Zanella, R. Cingolani, L. Manna, Assembly of colloidal semiconductor nanorods in solution by depletion attraction. Nano Lett. **10**, 743–749 (2010)
162. A. Gole, C.J. Murphy, Biotin–Streptavidin-induced aggregation of gold nanorods: tuning rod–rod orientation. Langmuir **21**, 10756–10762 (2005)
163. K. An, N. Lee, J. Park, S.C. Kim, Y. Hwang, J.-G. Park, J.-Y. Kim, J.-H. Park, M.J. Han, J. Yu, T. Hyeon, Synthesis, characterization, and self-assembly of pencil-shaped CoO nanorods. J. Am. Chem. Soc. **128**, 9753–9760 (2006)
164. B.P. Khanal, E.R. Zubarev, Rings of nanorods. Angew. Chem. Int. Ed. **46**, 2195–2198 (2007)
165. B. Ye, G. Qian, X. Fan, Z. Wang, Self-assembled superlattices from colloidal TiO_2 nanorods. Curr. Nanosci. **6**, 262–268 (2010)
166. A. Ghezelbash, B. Koo, B.A. Korgel, Self-assembled stripe patterns of CdS nanorods. Nano Lett. **6**, 1832–1836 (2006)
167. S.A. Maier, M.L. Brongersma, P.G. Kik, S. Meltzer, A.A.G. Requicha, H.A. Atwater, Plasmonics—a route to nanoscale optical devices. Adv. Mater. **13**, 1501–1505 (2001)
168. M.S. Gudiksen, K.N. Maher, L. Ouyang, H. Park, Electroluminescence from a single-nanocrystal transistor. Nano Lett. **5**, 2257–2261 (2005)
169. K. Mitamura, T. Imae, N. Saito, O. Takai, Fabrication and self-assembly of hydrophobic gold nanorods. J. Phys. Chem. B **111**, 8891–8898 (2007)
170. L. Onsager, The effects of shape on the interaction of colloidal particles. Ann. NY. Acad. Sci. **51**, 627–659 (1949)
171. D. Frenkel, H.N.W. Lekkerkerker, A. Stroobants, Thermodynamic stability of a smectic phase in a system of hard rods. Nature **332**, 822–823 (1988)
172. A. Singh, H. Geaney, F. Laffir, K.M. Ryan, Colloidal synthesis of Wurtzite Cu_2ZnSnS_4 nanorods and their perpendicular assembly. J. Am. Chem. Soc. **134**, 2910–2913 (2012)
173. A. Singh, C. Dickinson, K.M. Ryan, Insight into the 3D architecture and quasicrystal symmetry of multilayer nanorod assemblies from Moiré interference patterns. ACS Nano **6**, 3339–3345 (2012)
174. Z. Zhang, H. Sun, X. Shao, D. Li, H. Yu, M. Han, Three-dimensionally oriented aggregation of a few hundred nanoparticles into monocrystalline architectures. Adv. Mater. **17**, 42–47 (2005)
175. J. Zhuang, A.D. Shaller, J. Lynch, H. Wu, O. Chen, A.D.Q. Li, Y.C. Cao, Cylindrical superparticles from semiconductor nanorods. J. Am. Chem. Soc. **131**, 6084–6085 (2009)
176. T. Wang, J. Zhuang, J. Lynch, O. Chen, Z. Wang, X. Wang, D. LaMontagne, H. Wu, Z. Wang, Y.C. Cao, Self-assembled colloidal superparticles from nanorods. Science **338**, 358–363 (2012)
177. Z.-C. Xu, C.-M. Shen, C.-W. Xiao, T.-Z. Yang, S.-T. Chen, H.-L. Li, H.-J. Gao, Fabrication of gold nanorod self-assemblies from rod and sphere mixtures via shape self-selective behavior. Chem. Phys. Lett. **432**, 222–225 (2006)